Global and Planetary Change 265 (2026) 105589

Contents lists available at ScienceDirect

Global and Planetary Change

journal homepage: www.elsevier.com/locate/gloplacha

Climate-extreme-driven genesis of a Cretaceous dinosaur *Lagerstätte*

Federico Fanti [a,b,1], Lorenzo Consorti [c], Marco Muscioni [a,b], Lorenzo Baldassari [a], Enrico Dinelli [a], Maurizio Polentarutti [d], Giorgio Bais [d], Alexander Farnsworth [e,f], Evelyn Kustatscher [g], Amalia Spina [h], Alfio Alessandro Chiarenza [i,j,1,*]

[a] *Dipartimento di Scienze Biologiche, Geologiche e Ambientali, Alma Mater Studiorum Università di Bologna, via Zamboni 67, 40126 Bologna, Italy*
[b] *Collezione di Geologia 'Museo Giovanni Capellini', Alma Mater Studiorum Università di Bologna, via Zamboni 63, 40126 Bologna, Italy*
[c] *Istituto di Scienze Marine, Consiglio Nazionale delle Ricerche (CNR-ISMAR), Area Science Park, S.S 14 Km 163.5 Basovizza, Edificio Q2, 34149 Trieste, Italy*
[d] *Elettra Sincrotrone Trieste, Area Science Park, S.S. 14 Km 163.5, Basovizza, 34149 Trieste, Italy*
[e] *School of Geographical Sciences and Cabot Institute for the Environment, University of Bristol, Bristol, UK*
[f] *State Key Laboratory of Tibetan Plateau Earth System, Environment and Resources (TPESER), Institute of Tibetan Plateau Research, Chinese Academy of Sciences, Beijing, China*
[g] *Department of Natural History, Collection and Research Centre (SFZ), Tiroler Landesmuseen, Hall in Tirol, Austria*
[h] *Dipartimento Di Fisica e Geologia, Università di Perugia, Via Pascoli, 06123 Perugia, Italy*
[i] *Department of Earth Sciences, University College London, Gower Pl, WC1E 6BS London, UK*
[j] *North Carolina Museum of Natural Sciences, Raleigh, NC, USA*

ARTICLE INFO

Editor: Dr. Haijun Song

Keywords:
Exceptional fossil preservation
Dinosauria
Crocodylomorpha
Arthropoda
Plants
Italy

ABSTRACT

Konservat-Lagerstätten provide exceptional records of past ecosystems, yet the environmental and climatic processes governing their formation in extreme climatic regimes remain a significant, unresolved conundrum. Here we present a novel, process-based mechanism for the Villaggio del Pescatore *Konservat-Lagerstätte* (northeastern Italy; Late Cretaceous, 80 Ma), which preserves a diverse terrestrial and aquatic biota. Integrating high resolution synchrotron micro-analyses, bulk geochemistry, detailed taphonomy and palaeoclimate simulations we identify a dynamic, monsoon-paced tidal flat ecosystem within a carbonate coastal margin. Field and core records comprise metrescale packages of laterally persistent light–dark laminae; microstratigraphic, spectral and statistical analyses indicate a semidiurnal tidal regime with neap–spring modulation. MicroXRF/XRD mapping reveals that individual microlaminae within couplets share the same elemental inventory refuting a seasonal varve origin. Laminae chronometry, tied to the tidal interpretation, constrains net accumulation of the fossil bearing rhythmites to decadal (~40 year) timescales. Geochemical proxies record alternating terrigenous rich, high TOC intervals and drier, better oxygenated intervals. Palaeoclimate model ensembles diagnose a vigorous, summer dominated monsoon domain at ~29° N under greenhouse boundary conditions. We document that episodic monsoon enhanced flood and tropical cyclone pulses delivered sediment, nutrients, carcasses and plant debris to a microbially active, carbonate tidal flat; microbial mats rapidly stabilised and promoted early cementation, enabling exceptional soft tissue preservation. We propose a genetic model in which monsoon–cyclone forcing, tidal trapping and microbial sealing combine to produce decadal, daily resolved vertebrate *Lagerstätten* in greenhouse settings, offering predictive targets for similar deposits and deep time analogues for modern coastal change.

1. Introduction

Konservat-Lagerstätten preserve exceptional snapshots of past ecosystems, yet the event-scale environmental and climatic mechanisms that generate such deposits in extreme regimes remain poorly constrained. While *Lagerstätten* are invaluable for reconstructing palaeoecology and evolutionary history (Allison, 1988; Allison and Briggs, 1993; Muscente et al., 2017; Kimmig and Schiffbauer, 2024; Woolley et al., 2024; Varejão et al., 2025), they are rare in humid, low-latitude settings where rapid decay and active biotic processes normally

* Corresponding author.
E-mail addresses: federico.fanti@unibo.it (F. Fanti), a.chiarenza15@gmail.com, alfio.chiarenza@ucl.ac.uk (A.A. Chiarenza).
[1] Both authors equally contributed to this manuscript.

https://doi.org/10.1016/j.gloplacha.2026.105589
Received 27 February 2026; Received in revised form 21 June 2026; Accepted 24 June 2026
Available online 4 July 2026
0921-8181/© 2026 The Authors. Published by Elsevier B.V. This is an open access article under the CC BY license (http://creativecommons.org/licenses/by/4.0/).

preclude exceptional preservation (Retallack, 1990a, 1990b; Rosas et al., 2022). In modern, low-latitude, tropical coastal settings, monsoon systems and associated tropical cyclones drive much of the freshwater, sediment and nutrient flux, delivering short-lived but high-magnitude pulses that reshape shorelines and ecosystems. In the geological record, however, such extreme meteorological events are often time-averaged (Farnsworth et al., 2019); thus, most reconstructions of monsoon strength and seasonality rely on regional, time-averaged proxies rather than high-resolution archives that record single events (e.g., individual cyclones or discrete hyperpycnal floods). Coastal paralic carbonates and tidal flats are among the few settings that can generate these taphonomic 'sweet spots': they record complex depositional changes driven by low– to very high amplitude sea-level oscillations, and during transgression carbonate sediment is reworked across subaerially exposed substrates, creating a patchwork of small, hydrologically diverse settings (Allen et al., 1990). Within this mosaic, tidal flats on carbonate platforms stand out as particularly effective archives, because their broad surfaces with poorly developed soils and tables favour early diagenesis which, in strongly seasonal climates, can coincide with rapid burial and thus exceptional preservation (Noto, 2010).

The Villaggio del Pescatore (VdP) site lies within Upper Cretaceous–Palaeogene carbonate platform deposits near the village of Duino Aurisina (Trieste, north-eastern Italy). These strata formed part of the northern Adriatic Carbonate Platform (AdCP), a broad palaeogeographic domain extending from the present-day western Balkans to north-eastern Italy (Vlahović et al., 2005). VdP is one of the most informative Late Cretaceous fossil localities in the Mediterranean region: fossils documenting a diverse coastal and terrestrial biota are concentrated in a laterally restricted lens of slumped, finely laminated carbonate rhythmites (Palci, 2003; Consorti et al., 2021). This lens constitutes a vertebrate *Konservat-Lagerstätte* preserving articulated dinosaurs, crocodylians, teleost fishes, palaemonid arthropods and plants, with frequent soft-tissue outlines and microbial fabric traces (Dalla Vecchia, 2009; Chiarenza et al., 2021; Muscioni et al., 2023; Muscioni et al., 2025a; Muscioni et al., 2025b). Previous interpretations ranged from seasonal varves in a restricted, insular basin (Arbulla et al., 2006), to tectonically controlled brackish depressions (Tarlao et al., 1993), and a sinkhole–cenote models (Dalla Vecchia, 2020). Given the prevalence of tidal flats on the Upper Cretaceous AdCP system (Diedrich et al., 2011; Frijia et al., 2015; Spalluto et al., 2025), we here apply a process-based, multi-proxy reappraisal to test these competing hypotheses. Using an integrative framework – high-resolution synchrotron micro-analyses, bulk geochemistry, taphonomic study and palaeoclimate modelling – we resolve individual laminae and lamina sets showing that the VdP rhythmite lens accumulated on a dynamic, monsoon-paced tidal flat subject to semidiurnal tides and neap-spring modulation. Lamina chronometry tied to this tidal interpretation, together with independent taphonomic evidence for rapid burial of large vertebrates (e.g. dinosaurs and crocodylians), constrains net accumulation of the fossil-bearing rhythmites to decadal (~40 yr) timescales, uniquely resolving deposition and preservation at event-scale resolution. Comparable dark, finely laminated carbonate successions across the wider Adriatic region therefore constitute a valuable archive for reconstructing palaeoenvironmental conditions, terrestrial–marine linkages and sequence stratigraphic architecture under greenhouse climates, and the VdP record provides a process-based framework for interrogating these deposits and informing models of coastal evolution in modern analogue settings.

Our results identify a process linkage, including monsoon-enhanced flooding, tidal trapping and microbial sealing, that can generate exceptional vertebrate *Lagerstätten* in low-latitude, carbonate-dominated greenhouse settings.

2. Geological setting at VdP

At Villaggio del Pescatore (Fig. 1), the lower part of the exposed succession comprises the *Aurisina* facies (*Aurisina* limestone; Chiarenza et al., 2021), a series of alternating wackestones and high-energy shoal deposits (bioclastic packstones–grainstones rich in rudists, benthic foraminifera, echinoderm, red algae and cyanobacterial aggregates). The fossiliferous lens overlies the *Aurisina* facies, extends ~70 m laterally, and attains a preserved thickness of ~14 m (Fig. 1C), corresponding to the logged laminated succession used for the chronometric calculations in Section 4.1. The lens consists of finely laminated, dark–light brown carbonate rhythmites interbedded with carbonate breccias. The contact between the *Aurisina* limestones and the Liburnian-type rhythmites is a prominent, heavily karstified surface related to subaerial exposure originated by the Dinaric forebulge uplift. Regionally, this surface is correlated to the lower middle Campanian (Tentor et al., 1995; Steuber et al., 2005; Vlahović et al., 2005; Jurkovšek et al., 2016; Consorti et al., 2017; Chiarenza et al., 2021; Consorti et al., 2021). At VdP, the basal contact comprises three juxtaposed intervals: (a) undisturbed *Aurisina* limestone; (b) an epikarstic surface overlain by 20–50 cm of alluvial calcrete/breccia; and (c) the onset of dark, Liburnian-type millimetre-thick rhythmites of very fine-grained laminated carbonate mud. Correlative sections near Kozina (Slovenia) show karstified *Aurisina* beds forming a rugged palaeotopography infilled by reworked material, including bones (Debeljak et al., 2002) and capped by laminated carbonates, demonstrating that the laminated unit onlaps this irregular relief. The fossiliferous interval at the site is characterised by a finely laminated carbonate succession displaying exceptional microstratigraphic continuity. Detailed field observations and high-resolution photographic documentation reveal that the interval is composed of beds internally organised into millimetre – to sub-millimetre – scale laminae. Macroscopic logging at VdP (Fig. 1) identifies two main lamina sets, dark and light, arranged in metre-scale packages: a basal dark interval (0–6.0 m), an overlying light interval (6.0–7.6 m) and an upper dark interval (7.6–14 m) all characterised by short-lived colour variations. The uppermost ~4 m of the succession includes underwater slumps ranging from centimetres to >1 m thick. Microscale analyses of continuous cores (S1–S4) and recovered slabs show that the undisturbed portions of the laminated unit are composed of laterally continuous micro-couplets (dark–light) 0.31–0.69 mm thick. These laminae contain sparse mm-sized carbonate grains and are intercalated with millimetre – to centimetre-scale –debris-flow beds composed of reworked *Aurisina* clasts and bioclasts. Previous work interpreted these rhythmites as varves, with each couplet representing a seasonal pair (thin dark micro-lamina = rainy season; thicker light micro-lamina = dry season) (Arbulla et al., 2006). However, our high-resolution synchrotron analyses (presented in Section 4.2, Geochemical Signatures) reveal that individual micro-laminae within couplets share an identical elemental assemblage, varying only in relative abundance rather than distinct chemical composition, thereby refuting a classical seasonal varve genesis.

3. Methods

All samples for lithological, sedimentological and taphonomic analyses were sampled at Villaggio del Pescatore, Trieste, Italy (45.8° N, 13.6° E) including continuous cores from the site. Detailed methodological and instrument settings for analyses are reported in SI.

3.1. Sampling and lamina measurements

High-resolution petrographic and geochemical analyses were carried out on laminated limestones from the Villaggio del Pescatore (VdP) core S3, archived at the University of Trieste (Palci, 2003). Four bulk samples (VPC1–VPC4) and six thin sections (VP12, VP15, VP21, VP27, A1, B1) were selected to represent the main dark and light lamina packages

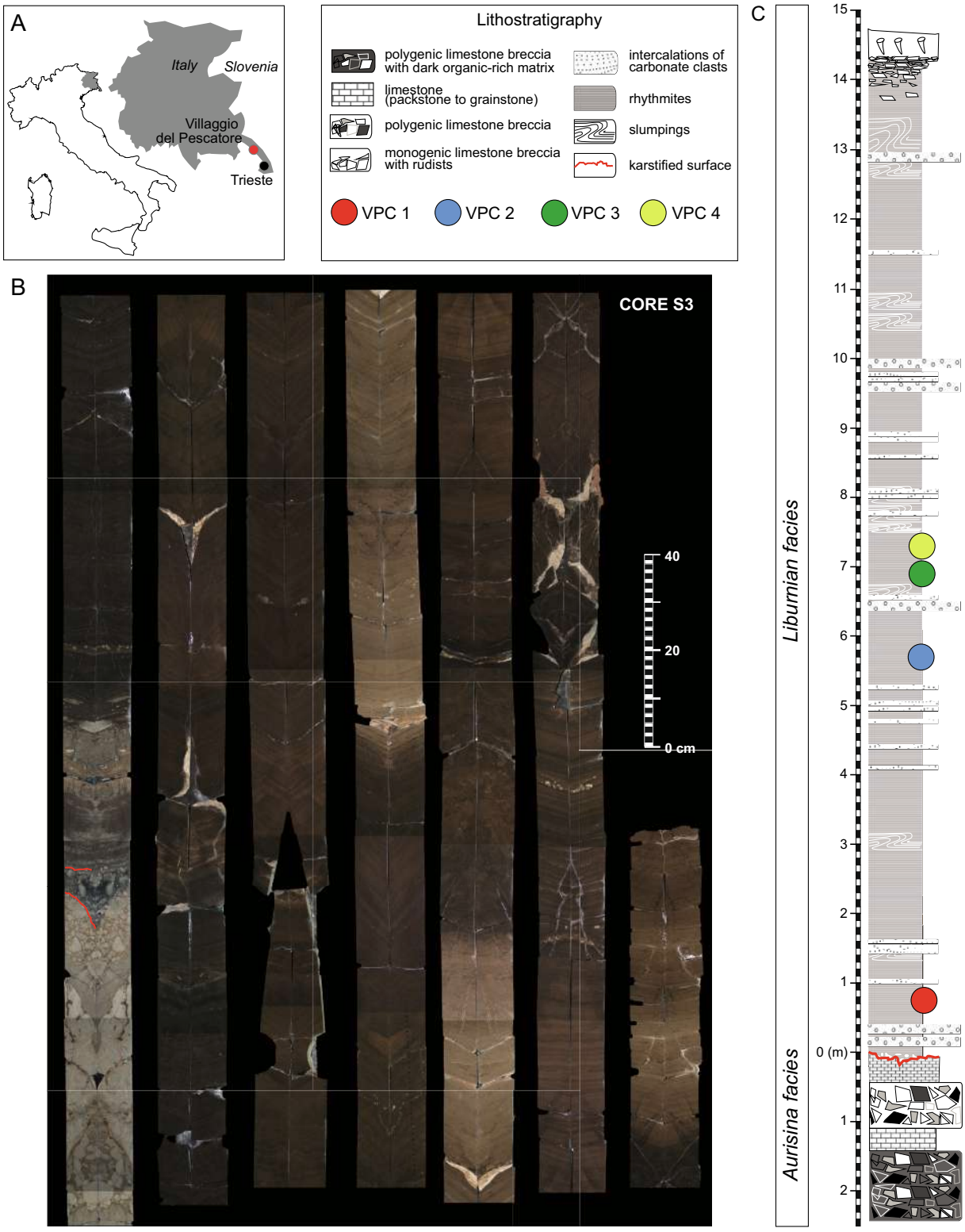

Fig. 1. High-resolution stratigraphy and sampling framework of the Villaggio del Pescatore (VdP) laminated interval. (A) Geographic location of the VdP locality in northern Italy (near Trieste). (B) Composite photographic log of Core S3, aligned with the stratigraphic column, showing the physical expression of the rhythmites and event horizons discussed in the text. (C) Detailed stratigraphic log of the fossiliferous lens, illustrating the vertical distribution of distinct light and dark lamina packages, the stratigraphic position of episodic event beds (debris flows), and intervals affected by soft-sediment deformation (slumps). The precise stratigraphic horizons for bulk geochemical samples (VPC1–VPC4) and corresponding thin sections (VP12, VP15, VP21, VP27, A1, B1) are indicated to cross-reference with geochemical and micro-textural data.

(Fig. 3). Micro-lamina thicknesses were measured on calibrated high-resolution images in ImageJ along multiple, co-oriented transects to assess precision. These measurements underpin lamina-scale statistics and the couplet-to-time calibration used to derive depositional rates and tidal cyclicity. Our chronological framework is established through a precise hierarchical definition of depositional units. A lamina represents a single depositional event, observed as either a light or dark-coloured layer. Multiple such laminae form lamina sets. The fundamental unit for our high-resolution temporal analysis is the couplet, defined as one light and one dark lamina. Under a semidiurnal tidal interpretation (two similar high and low tides per day), we adopt the working assumption that two couplets, comprising four laminae (light-dark-light-dark), represent one solar day (Kvale et al., 1995). Given the homogeneity and continuity of the rhythmites, this mapping is internally consistent. This daily resolution then allows for the characterisation of rhythmites, which are generic intervals or packages of these laminated limestones, collectively forming the VdP fossil lens.

3.2. Synchrotron micro-XRF and micro-XRD

Synchrotron-based micro-XRF and micro-XRD were performed in parallel at the XRD1 beamline of the Elettra facility (Trieste, Italy) on 10 samples (VPC1–4, VP12, VP15, VP21, VP27, A1, B1). Line scans were acquired perpendicular to lamination using a focused micrometre-scale X-ray beam and 50–100 μm spacing, yielding 75–200 analyses per thin section. Two-dimensional diffraction patterns were integrated and compared with reference patterns (Crystallography Open Database, PDF4) to identify mineral phases. XRD patterns showing only calcite peaks, together with CaO-dominated bulk compositions, indicate that the VdP laminites are overwhelmingly calcitic and formed in a dominantly carbonate depositional system.

Micro-XRF elemental maps were co-registered to lamina-thickness transects, allowing one-to-one comparison between individual micro-laminae and elemental variability (dark–light). At the couplet scale, dark and light micro-laminae contain the same elemental assemblage, with differences limited to relative abundances, whereas consistent contrasts occur between multi-decimetre packages of darker and lighter lamination. Full beamline settings and data-reduction procedures are provided in the Supplementary Information.

3.3. Bulk geochemistry and loss-on-ignition

Sixteen subsamples were cut at ~1.5 cm intervals from the laminated unit, powdered and analysed by wavelength-dispersive X-ray fluorescence (WD-XRF) at the Department of BiGeA, University of Bologna. Pressed tablets were measured using a PANalytical AXIOS 4000 spectrometer, yielding major-element concentrations (reported as oxides, wt %) and trace-element abundances (ppm). Concentrations <5 ppm were treated as unreliable and excluded from interpretation. Loss on ignition (LOI) was determined by heating powders to 950 °C overnight.

Ba–Rb–Sr ternary diagrams were used to infer relative salinity and depositional setting following established schemes, placing the laminites between marginal-marine and inland freshwater fields, with a bias towards marginal-marine conditions (Zhang et al., 2017; Rosatelli et al., 2023). Major-element data show that CaO, SiO_2 and SO_3 are the principal components, with MgO and Al_2O_3 generally above 1 wt% and all other oxides <1 wt%. CaO increases upwards from VPC1 to VPC3–4, whereas MgO and SO_3 decrease. Among trace elements, Sr and Cl are the most abundant; Sr is enriched in VPC1 relative to VPC2–4, and Zr is likewise enriched in VPC1, consistent with higher basal terrigenous input. LOI values are relatively homogeneous (42.96–43.94 wt%) and exceed those expected for stoichiometric calcite at a given CaO content, indicating that a fraction of the volatile mass derives from components other than pure $CaCO_3$. Analytical protocols, detection limits and calibration procedures are reported in the Supplementary Information.

3.4. Geochemical proxies

Bulk WD-XRF and LOI data were used to reconstruct terrigenous input, palaeoproductivity and palaeoclimatic humidity at the scale of lamina packages. Following Engelke et al., 2018, Grabowski et al., 2021, Godet et al., 2023, and Lodowski and Grabowski, 2023, we calculated "excess" values (X_ex) to separate non-terrigenous contributions from detrital input, using Al_2O_3 as a terrigenous proxy (Hetzel et al., 2011; Godet et al., 2023) and average shale compositions from Wedepohl (Wedepohl, 1971). The terrigenous fraction was estimated using TiO_2-normalised indices. Details of the equations and parameter choices are given in the Supplementary Information.

At the micro-lamina scale, where WD-XRF and LOI were not feasible, micro-XRF fluorescence intensities were treated as semi-quantitative proxies for relative concentration changes, assuming linearity between counts and concentration for a given element.

Palaeoproductivity was assessed using Sr/CaO (ppm/wt% CaO) as a carbonate-normalised proxy for relative coccolithophore input to bulk carbonate (Stoll and Bains, 2003; Fornaciari et al., 2007; Engelke et al., 2018). We emphasise stratigraphic trends within VdP rather than absolute comparisons with other basins, because diagenetic modification is known to affect Sr in calcite (Palci, 2003; Ando et al., 2006). Additional proxies for terrigenous input (e.g. Zr/Al_2O_3, MgO/Al_2O_3, Cr/Al_2O_3) and humidity/chemical weathering (Al_2O_3/K_2O, TiO_2/K_2O) were applied following the same literature.

3.5. Modern tropical-cyclone analogues

Interpretation of flood and event beds at VdP draws on process analogues from modern tropical-cyclone–affected coasts where hurricanes and typhoons generate short-lived, high-magnitude sediment and freshwater pulses. These systems show characteristic signatures of TC impact, including sediment-laden river plumes, hyperpycnal flows, storm-bed couplets on tidal flats, and terrestrial-rich event layers identified by grain-size profiles, organic-matter composition and elemental ratios (e.g. Zr/Ti, Ti/Al). We use these observations to interpret the VdP debris-flow beds, terrigenous geochemical enrichments and the alternation of storm-derived event layers with tidally laminated carbonates.

3.6. Palaeoclimate modelling

Campanian palaeoclimate simulations were performed with the Hadley Centre coupled and atmosphere-only models (HadCM3L and HadAM3B) using alternative palaeogeographic reconstructions (including Scotese palaeogeographies (Scotese and Wright, 2018; Scotese, 2021)) and proxy-derived CO_2 trajectories appropriate for Late Cretaceous greenhouse conditions. Monsoon domains were diagnosed using the Wang & Ding (Wang and Ding, 2008) global monsoon criterion and a monsoon precipitation index (MPI) based on seasonal contrasts in precipitation. For each configuration, we extracted seasonal precipitation, MPI and monsoon masks for grid cells corresponding to the northern Adriatic Carbonate Platform and the VdP region. Additional sensitivity experiments varied the extent of emergent land in the Adriatic–Dinaric sector to test the impact of landmass size on monsoon strength and continuity. Model setup, boundary conditions and diagnostic definitions are described in detail in the SI.

4. Results

4.1. Lithological and stratigraphic evidence for tidal rhythmites at Villaggio del Pescatore

At VdP, the lamination consists of a systematic alternation of light-coloured and dark-coloured laminae (Figs. 2–4). Light laminae are dominated by fine-grained carbonate mud, exhibiting homogeneous texture and sharp upper and lower boundaries. Dark laminae are

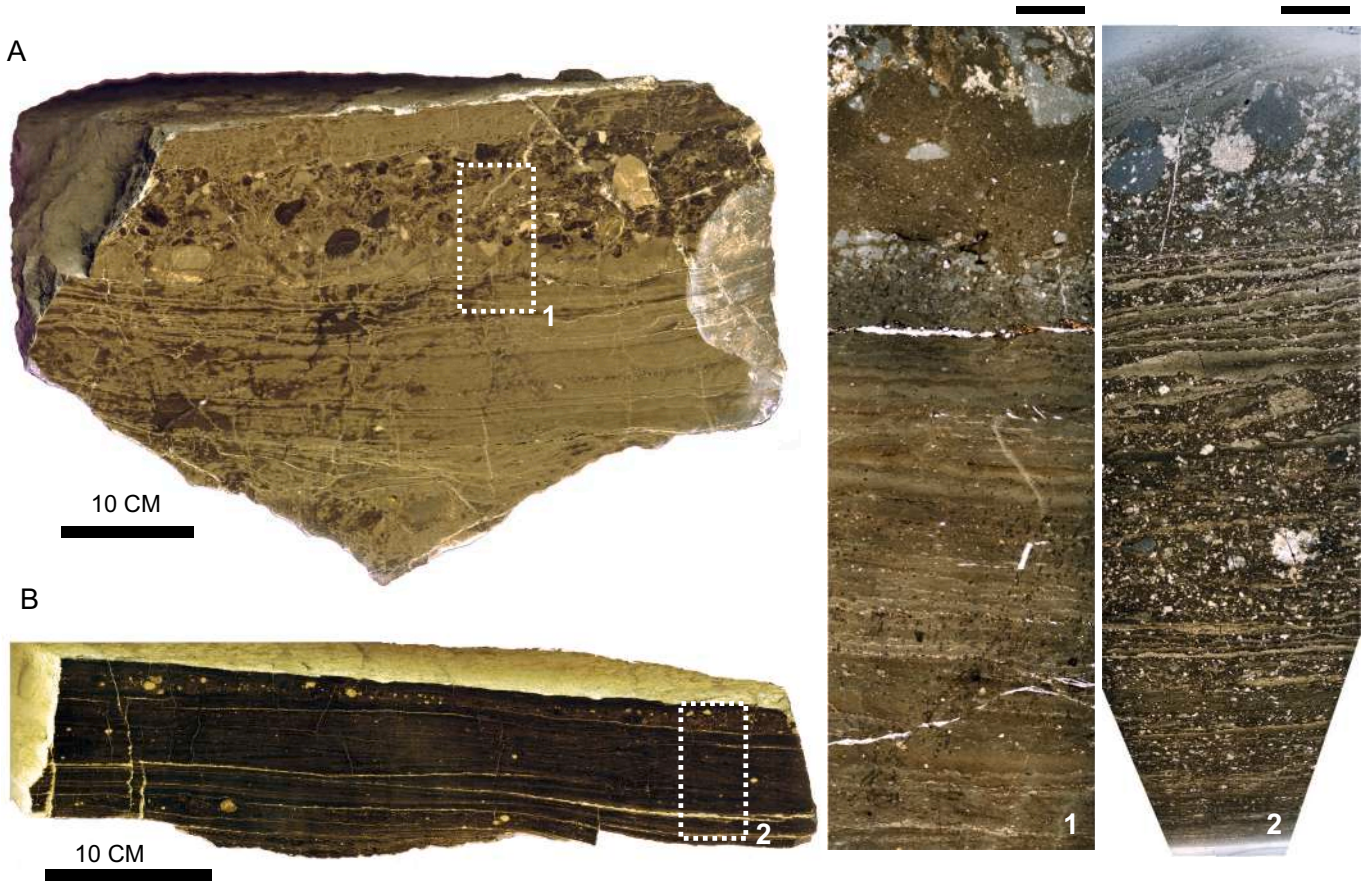

Fig. 2. VdP rhythmites cyclicity in light-coloured and dark-coloured sets of laminae. Representative bulk samples documenting the distinct lithological characteristics within light-coloured (A), and dark-coloured (B) lamina packages at the Villaggio del Pescatore site. Both samples demonstrate the rhythmic alternation of laminated background sedimentation with episodic, high-energy event beds (clast-dominated flows). Microphotographs shown in (C) and (D) highlight the sharp lithological transition from finely laminated carbonate rhythmites to clast-dominated flow deposits containing reworked *Aurisina* and Liburnian clasts/pebbles.

comparatively thinner and enriched in fine detrital material, imparting a darker tone and locally enhanced opacity (Fig. 2). This rhythmic alternation is laterally persistent, indicating deposition under uniform conditions rather than localised sedimentary reworking. Importantly, individual laminae show no evidence of internal erosion, truncation, or amalgamation. Contacts between successive laminae are sharp but non-erosive. Bioturbation is entirely absent throughout the laminated interval, both at outcrop scale and in close-up imagery, indicating rapid burial and conditions unfavourable to benthic reworking. Microstratigraphic stacking patterns reveal that laminae are organised into discrete lamina sets, each comprising several light–dark couplets bounded by subtle but laterally continuous surfaces. These bounding surfaces do not represent exposure or erosional discontinuities but instead mark slight changes in lamina thickness and composition, consistent with shifts in depositional intensity rather than interruption of sedimentation. The internal architecture of these lamina sets suggests repeated depositional pulses rather than continuous background accumulation. The thickness of individual laminae typically ranges from a few tenths of a millimetre to approximately one millimetre, with limited vertical variability. Our subsequent geochemical analyses (Section 4.3) reveal that individual micro-laminae within couplets share an identical elemental assemblage, varying only in relative abundance rather than distinct chemical composition, thereby refuting a seasonal varve origin.

To assess cyclicity, we measured successive laminae (excluding debris beds). Two hundred and thirty consecutive laminae from a dark interval yield an average couplet thickness of 0.28 mm ($n = 230$; see Methods). Additional intervals show mean couplet thicknesses of ~0.46 mm (dark interval) and ~ 0.56 mm (light interval). Scatter plots of successive lamina thicknesses, following established approaches for tidal rhythmites (Kvale et al., 1995), reveal signals associated with diurnal inequality, though variation in runoff strongly overprints the tidal signal. Nonlinear and spectral analyses favour a semidiurnal regime with neap–spring and longer-period (tropical-month) modulation.

Under a semidiurnal interpretation (two similar high and low tides per day), we adopt the working assumption that two couplets record one solar day (four laminae = two couplets = one day; see Methods) (Kvale et al., 1995). Given the homogeneity and continuity of the rhythmites, this mapping is internally consistent. Based on a total preserved thickness of 14 m, we derive a cumulative depositional timescale of approximately 41 years for the fossil-bearing rhythmites, identifying VdP as a decadal-scale snapshot of a Cretaceous ecosystem. Using mean daily rates derived from lamina measurements, the darker lamina packages (12.4 m = 12,400 mm) accumulated over ~36.9 years at an average rate of 0.92 mm day^{-1} (12,400 mm / 0.92 mm day^{-1} ≈ 13,478 days ≈ 36.9 yr). The lighter lamina packages (1.6 m = 1600 mm) added ~3.9 years at an average rate of 1.12 mm day^{-1} (1600 mm / 1.12 mm day^{-1} ≈ 1429 days ≈ 3.9 yr). Allowing for centimetre-scale debris events, intervals of non-deposition, and slumped intervals – syndepositional underwater events ranging from centimetres to >1 m thick that locally reduce the preserved stratigraphic thickness – we estimate a conservative total accumulation time on the order of four decades.

These estimates rest on three principal assumptions: (a) each couplet reliably records a single tidal cycle (see SI Table 2 for individual lamina measurements); (b) hiatuses and erosion within the measured interval are minor relative to net deposition; and (c) debris events represent

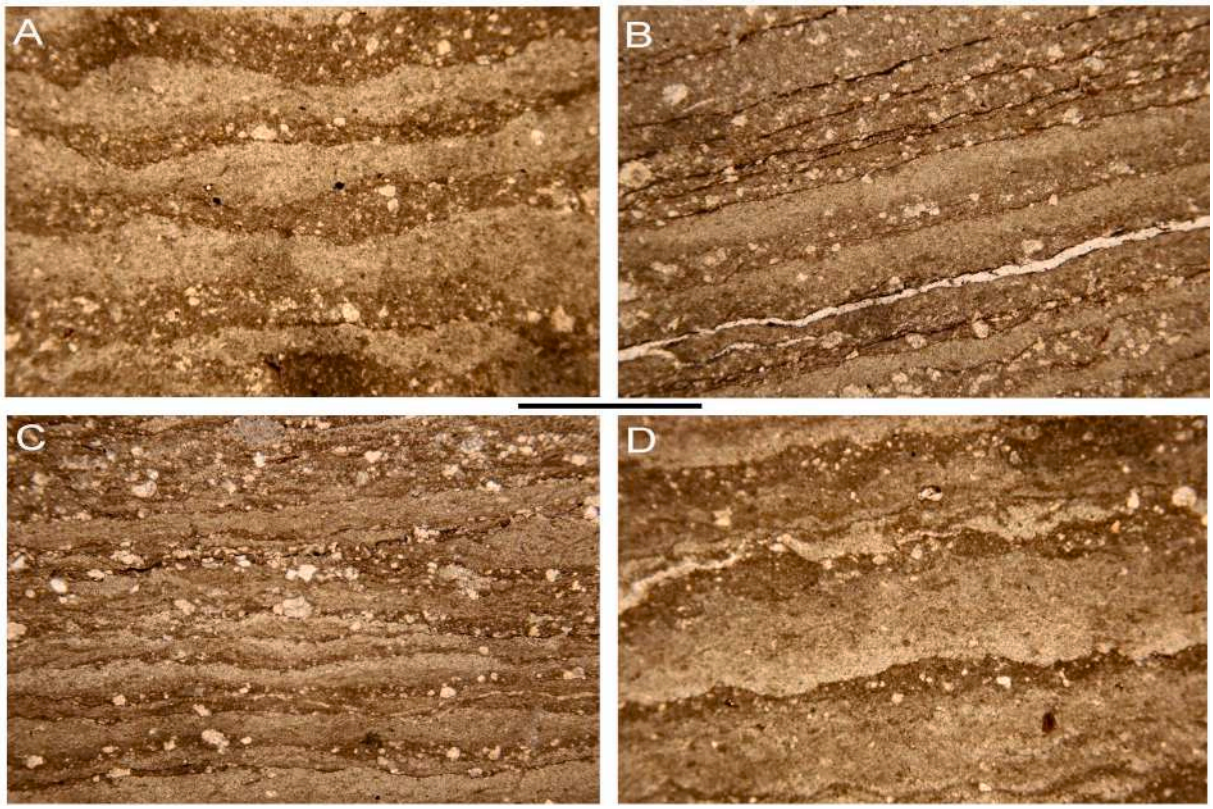

Fig. 3. Microstratigraphic characteristics of VdP laminated rhythmites from Core S3. Representative photomicrographs of thin sections from Core S3 illustrate the finely laminated nature of the VdP rhythmites, characterised by alternating light and dark laminae. (A, D) Light laminae, typically composed of fine-grained carbonate mud, show variable thickness often exceeding that of the associated dark laminae, which are enriched in fine detrital material. This variability reflects tidal influence and fluctuating sediment supply. (B, C) Panels display a relatively homogenous alternation of lighter and darker laminae. Note in panel (B) how lighter laminae are occasionally replaced by thin, reddish, residual-rich surfaces, possibly indicating localised oxidation or concentration of insoluble residues. The consistent lamina geometry, sharp contacts, and absence of bioturbation, coupled with evidence of draping, support rapid, incremental sedimentation and the pervasive influence of microbial stabilization during their emplacement. Scale bar: 1 mm for all panels.

effectively instantaneous deposits that do not substantially bias mean lamina thickness. If a diurnal regime were more appropriate, with one couplet rather than two per solar day, the inferred duration would approximately double to ~80 years, an alternative noted here for completeness but not supported by the microstratigraphic and spectral evidence presented.

This chronometry yields an average sediment accumulation rate of approximately 34 cm yr^{-1}, based on 14 m deposited over ~41 years. While this significantly exceeds the background accretion rates of typical, quiescent modern carbonate tidal flats (which generally range from millimetres to a few centimetres per year), it is highly consistent with modern coastal settings subjected to extreme, pulsed sediment supply. In modern tropical-cyclone and monsoon-impacted coasts (e.g., the Gulf of Mexico, the Caribbean, and Southeast Asian deltas; Rejmánek et al., 1988; Turner et al., 2006; Freeman et al., 2015; Furgerot et al., 2016; Clift and Jonell, 2021; Wang et al., 2021), single storm surges and associated hyperpycnal river floods can deposit decimetres of sediment in a matter of days. Furthermore, in macrotidal environments like the Bay of Mont-Saint-Michel, background accretion rates can also reach several tens of centimetres per year, demonstrating that high-energy, sediment-rich tidal systems provide an ideal physical template for rapid accumulation (Tessier et al., 2022 and references therein). At VdP, the combination of these high-magnitude sediment pulses, efficient trapping within a transgressive karst depression (increased accommodation space), and likely microbially mediated rapid stabilization allowed for these extraordinary, episodic accumulation rates to be preserved over decadal timescales.

The resulting decadal timescale for Early Campanian deposition is comparable to other well-preserved tidal rhythmites that record high-frequency, near-continuous sedimentation even on low-relief palaeotopographies (Kuecher et al., 1990; Steel et al., 2012). Diurnal or semidiurnal tidal models for the Late Cretaceous European shelf (Mitchell et al., 2010) indicate a micro – to mesotidal regime, with amplitudes of ~1–4 m for shallow-water carbonate platforms, including the AdCP.

Within the laminated intervals, the tidal sequences preserve micro debris-flow beds (0.2–1 cm) of reworked, relatively well-sorted carbonate clasts. Further, petrography of centimetre-thick debris-flow horizons that host large vertebrates shows that these beds incorporate coarse (≤2 cm), poorly sorted heterolithic clasts comparable to matrix-supported breccias. These layers have erosive traction bases and locally subaerial tops, and are overlain by draping, laminated carbonate. Clasts include reworked *Aurisina*-type or Liburnian-type carbonate, some bearing foraminifera and bivalve fragments, as well as semi-lithified rhythmite pebbles likely cannibalised from the local succession (*see* Chiarenza et al., SI 14).

Outcrop analysis and data from core S3 calibrated against the spatial and stratigraphic positions of all recovered fossils, identify four discrete large vertebrate-bearing horizons. Each coincides with major debris-rich event beds that interrupt an otherwise regular background of tidal lamination. These fossiliferous layers occur within both light and dark lamina packages. The sedimentary structures, textures, lithologies and vertical stacking pattern of the rhythmites support their interpretation as tidalites deposited on a carbonate-dominated, paralic

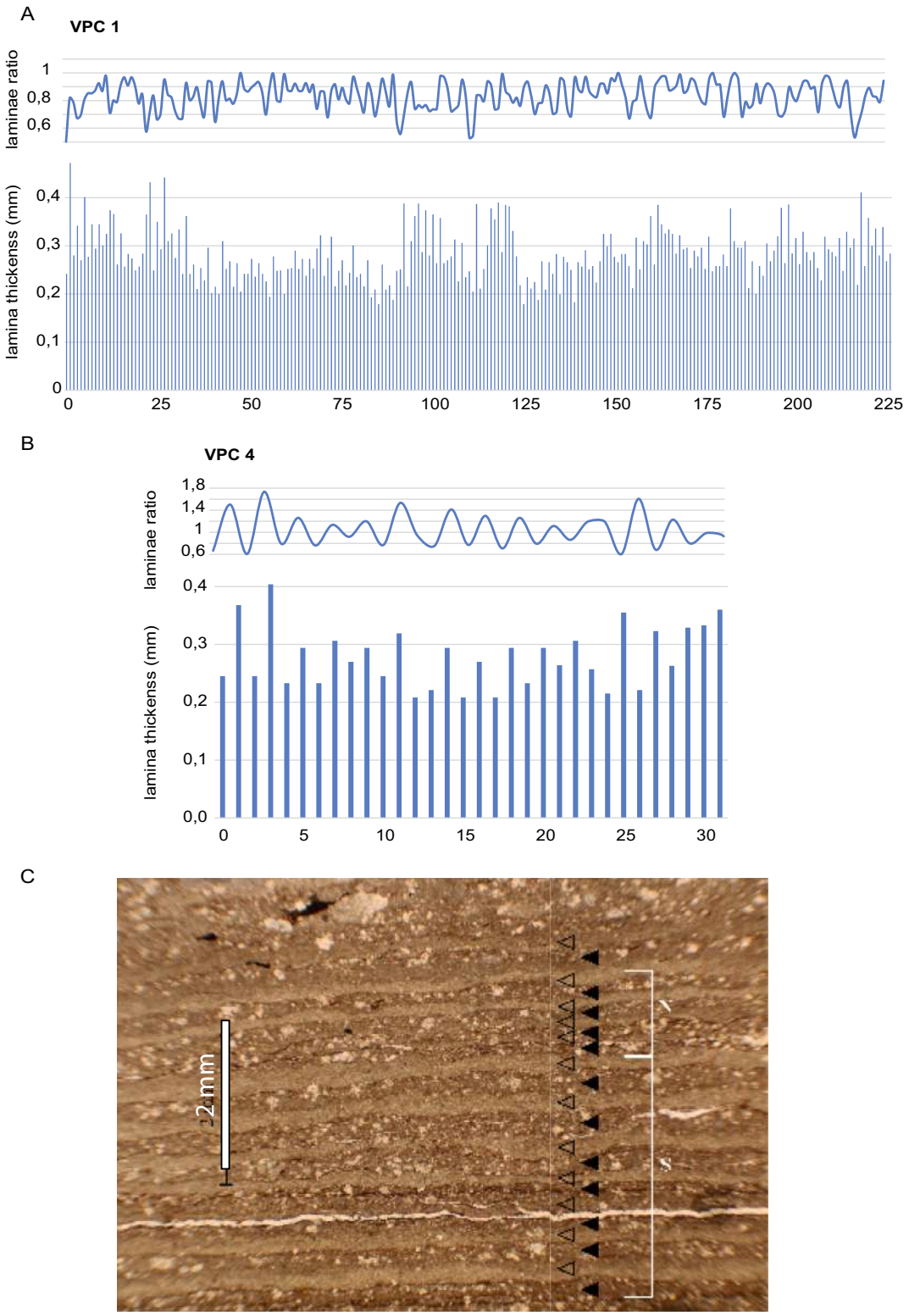

Fig. 4. Lamina Micro-Measurement & Cyclicity Analysis. (A) Representative single lamina thickness in mm (bottom) and relative diurnal inequality (top) measured on 230 dark laminae from core VPC1. (B) Representative lamina thickness in mm (bottom) and relative diurnal inequality (top) of 32 light laminae from core VPC4. Measurements were taken with ImageJ software based on high resolution micrographs of core sections. Higher number of measurements on darker VPC1 laminae is due to enhanced visibility between individual laminae, in contrast with the relative scarcity of values for VPC4. (C) Detail picture with relative measured sets of laminae.

subtidal–intertidal flat variably influenced by runoff. Packstone textures, near-continuous rhythmite accumulation, mixed clastic–bioclastic content and repeated debris flows are all compatible with such an environment. Locally consistent lamina thickness, and sequences of similarly sized couplets regularly followed by thicker or thinner sets, are interpreted as neap–spring tidal control (fortnightly synodic forcing). In tidal-flat settings, tidal fluctuations modulate water and sediment supply, modify local slopes and thresholds for debris-flow initiation, and

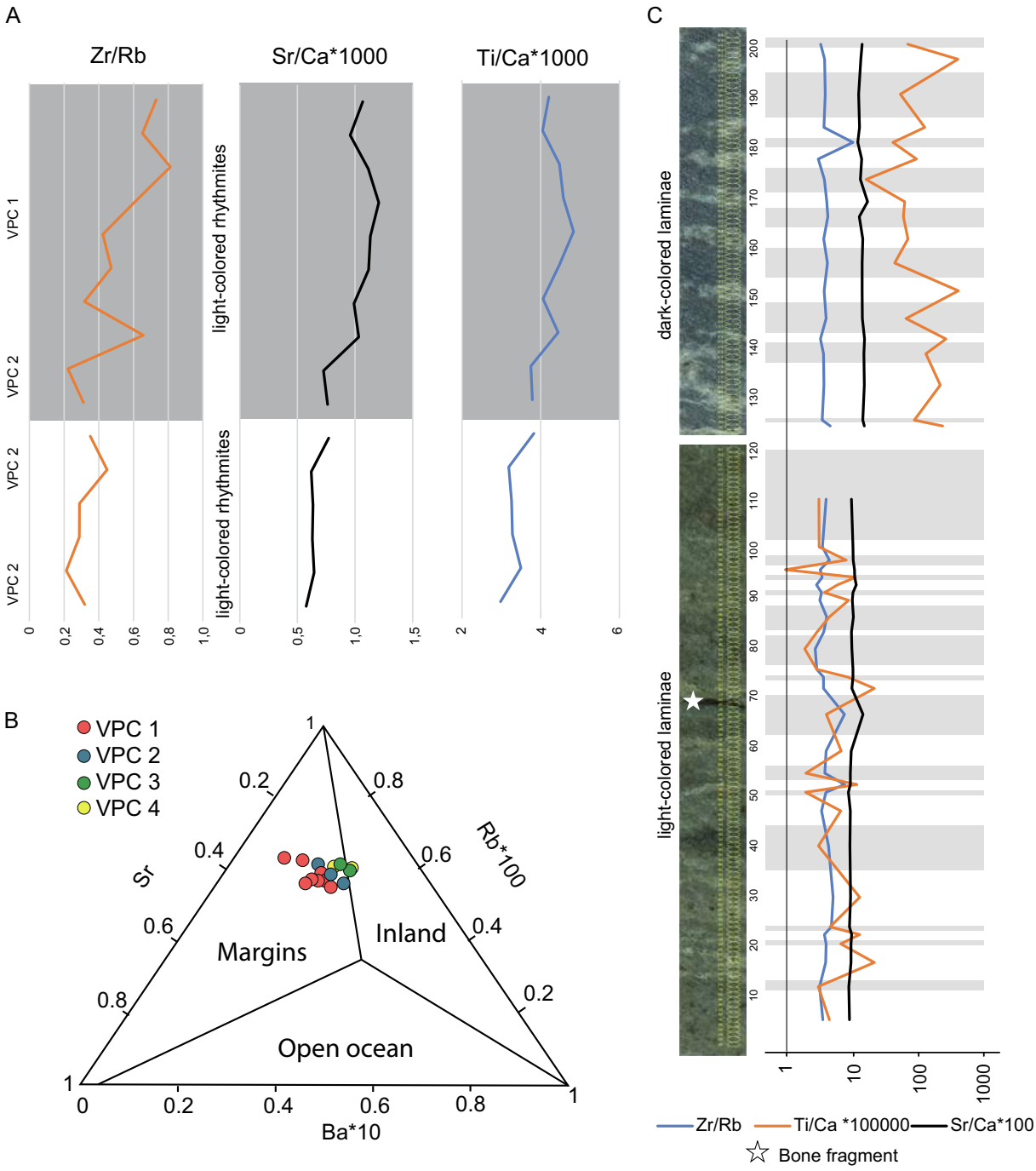

Fig. 5. Palaeoenvironmental and palaeosalinity proxies from VdP rhythmites. (A) profiles of key geochemical proxies (e.g., terrigenous input, productivity, redox indicators) from bulk samples of Core S3 (VPC1-VPC4). (B) Ba–Rb–Sr ternary diagram for the VdP carbonate-dominated deposits. (C) Mean elemental abundances of discussed proxies in light and dark lamina packages derived from Micro-XRF/XRD (50 μm step size) analyses.

efficiently record high-energy events produced by abrupt changes in continental discharge. At VdP, the micro debris-flow beds are interpreted as storm-tide deposits. We do not identify classic tempestites (wave-reworked, shoreward-transported storm beds) in the succession; deposits with tempestite-like appearance at VdP are demonstrably derived from terrestrial input (hyperpycnal/overwash and debris-flow deposits), although this does not preclude the local occurrence of true wave-generated tempestites elsewhere in the platform. The thicker debris-flow horizons that host transported multi-metre carcasses and plant debris are interpreted as products of rapid, large-scale inland flooding, potentially linked to intense seasonal storms (tropical-cyclone-style events). Such high-intensity, localised rainfall would strongly increase river discharge, alter coastal hydrodynamics and modify tidal propagation, promoting the combined runoff–tidal processes inferred here and creating the physical template for the subsequent exceptional fossil preservation.

4.2. *Geochemical proxies of the VdP palaeoclimate*

In classic varved successions, paired laminae typically display systematic differences in colour and chemistry (e.g. darker siliciclastic laminae versus lighter carbonate or biogenic laminae; Schimmelmann et al., 2016). While metre-scale packages of darker versus lighter laminae likely record changes in climate and sediment supply,

individual micro-laminae within couplets are distinguished in Ti/Ca, Rb/Ti and Zr/Ni values. Chemical weathering proxies (Al_2O_3/K_2O, TiO_2/K_2O) and palaeoclimate models for the uppermost Cretaceous (Křížová et al., 2024; O'Brien et al., 2017) indicate strengthening atmospheric circulation and enhanced cyclone/monsoon activity at the VdP's reconstructed subtropical palaeolatitude (Chiarenza et al., 2021; Chiarenza et al., 2022; Chiarenza et al., 2024) at ~29° N, 23° E. Within the Intertropical Convergence Zone, this region experienced strongly seasonal climates, even under greenhouse conditions, known to promote vertebrate preservation through seasonal flooding, high water tables, and rapid burial (Noto, 2010; Ziegler et al., 2003; Dubiel et al., 1991).

Bulk geochemical analysis reveals systematic contrasts between broader lamina packages. Although the mineralogy is dominated by calcite, darker lamina packages are characterised by a higher occurrence of silicate debris. This is suggested by elevated Ti/Ca ratios (Fig. 5) and similar increases in Si, Al, Fe, Mg, K, Cr, and Zr, which collectively indicate shifts in the siliciclastic input basinward, typically associated with intense continental runoff (Clift et al., 2014). However, these robust package-scale elemental contrasts are not replicated at the micro-lamina level. Parallel micro-XRF/XRD mapping at the Elettra Synchrotron (50/100 μm step size, $n = 200$ analyses, Table 1, SI) confirmed a calcite-dominated mineralogy with no systematic mineral phase changes across individual couplets. Crucially, dark and light laminae within a couplet share an identical elemental assemblage, varying only in relative abundance rather than distinct chemical composition. The optical darkness of individual micro-laminae within couplets likely reflects localised concentrations of organic matter or subtly finer grain sizes settled during periods of reduced hydrodynamic energy, rather than introducing qualitatively distinct chemical assemblages detectable at the micro-lamina scale. This strongly argues against a seasonal varve origin, supporting instead a tidal control on lamination. Nonetheless, the sequence records a continuous, albeit varying, terrigenous influx from runoff, aeolian input, and episodic discharge, primarily expressed at the broader package scale. For instance, Zr/Rb, a well-established grain-size proxy (Bassetti et al., 2016), decreases from VPC1 to VPC4, implying an overall fining-upward trend in mean grain size, which is also confirmed by the synchrotron data.

Organic matter data (Palci, 2003) reveal significantly higher TOC contents in darker lamina packages (0.48–0.84 wt%) compared to lighter ones (0.21–0.44 wt%), directly linking lamina colour to enhanced organic matter accumulation. This is further supported by high sulphur concentrations in dark lamina packages (1040–1950 mg/kg S) relative to light ones (480–510 mg/kg S). The sparse benthos and limited bioturbation observed in lighter beds indicate intervals of relatively improved oxygenation and more efficient organic degradation. Conversely, darker packages reflect more dysoxic conditions, which fostered the observed exceptional organic matter preservation. Palaeosalinity indicators, derived from Ba–Rb–Sr ternary diagram (Zhang et al., 2017), consistently position VdP's sediments between inland freshwater and marginal-marine fields, albeit with a clear bias towards marginal-marine conditions. This signature implies a highly dynamic depositional environment characterised by fluctuating salinity and variable marine influence, in line with a tidal flat subject to both marine tides and episodic freshwater discharge. Palaeoproductivity and carbonate producer input were tracked using Sr/Ca ratios and excess barium [Ba(ex)] (Paytan and Griffith, 2007). Elevated Sr/Ca, potentially reflecting increased coccolithophore contributions (Stoll and Bains, 2003; Guerreiro et al., 2024), suggests enhanced nutrient availability. Recognising that diagenesis complicates absolute comparisons (Palci, 2003), our analysis focused on internal stratigraphic contrasts. While absolute Ba(ex) values are generally lower than some Alpine limestones (Fornaciari et al., 2007) and align with recent Apennine records (Rosatelli et al., 2023), this contextualises the regional variability in productivity baselines. More importantly, multi-proxy trends within VdP show fluctuating productivity across VPC units: a modest increase in VPC1, higher values in VPC2, and subsequent decline or mixed signals in VPC3–4. Collectively, the geochemical datasets reveal a finely resolved picture of a paralic tidal-flat setting. Darker packages reflect humid, runoff-dominated periods, characterised by elevated terrigenous input, coarser grains, enhanced productivity (indicated by higher Sr/Ca and Ba(ex), Fig. 6), and less ossigenated bottom waters promoting exceptional organic matter preservation. Conversely, lighter packages indicate drier, more seasonal conditions, showing reduced terrigenous material, finer grains, lower TOC and sulphur, and improved oxygenation, with aeolian input becoming more prominent as runoff waned. Palaeosalinity indicators (Ba–Rb–Sr ratios; Zhang et al., 2017) further underscore this dynamic environment, positioning VdP's sediments between inland freshwater and marginal-marine fields, reflecting fluctuating salinity and variable marine influence. This dynamic interplay of monsoon-modulated freshwater discharge, episodic flood events, and fluctuating marine connectivity created the unique alternating states and distinctive chemical backdrop essential for the exceptional fossil preservation observed at VdP. We emphasise that these interpretations carry differing levels of confidence. The most robust signals are the internal, package-scale stratigraphic contrasts in detrital input and organic enrichment: the dark-versus-light contrasts and upward trends in Ti/Ca and related terrigenous ratios, the Zr/Rb grain-size proxy, and the covariation of TOC and sulphur. These signals rest on comparatively diagenesis-insensitive elemental ratios and are mutually consistent. By contrast, the productivity, salinity, and redox interpretations are more tentative and are presented as relative, within-section trends rather than absolute values. Sr/Ca and Ba(ex) are read only as qualitative indicators of changing carbonate-producer and nutrient flux, given the known diagenetic sensitivity of Sr in calcite (Section 4.2; Supplementary Section 3.1). The Ba–Rb–Sr ternary fields place VdP qualitatively between marginal-marine and freshwater end-members, rather than yielding quantitative palaeosalinity estimates. Similarly, the inference of alternating dysoxic and better-oxygenated bottom waters rests on indirect sedimentary and organic-geochemical evidence, including bioturbation intensity, TOC, and sulphur contents, rather than on dedicated redox-sensitive trace-metal proxies, which are difficult to apply unambiguously in carbonate-dominated settings. We therefore anchor our palaeoenvironmental model on the robust internal stratigraphic trends and treat the productivity, salinity, and redox proxies as consistent but supporting, qualitative lines of evidence.

4.3. Taphonomy

Taphonomic and sedimentological evidence at VdP imply extremely rapid sedimentation when considered cumulatively across the fossiliferous interval. Crucially, laminated carbonate strata drape fossil elements, including large vertebrates, without evidence of basal erosion or sediment bypass (Fig. 7). Laminae conform and even onlap to fossil surfaces, infilling interstitial spaces and maintaining continuity across skeletal margins. This geometry demonstrates that lamination postdates carcass emplacement and that burial occurred through incremental sediment accretion rather than single catastrophic burial events. The absence of disruption at the bone–sediment interface further indicates minimal post-depositional reworking. Many laminae drape the top surfaces of debris-flow beds, smoothing otherwise irregular topography. In modern tidal flats, similar draping occurs where mucous-rich cyanobacterial or microbial covers stabilise sediments through baffling and binding (Noffke et al., 2001; Gischler et al., 2008; Diedrich et al., 2011). Repeated growth and burial of benthic biofilms — including photosynthetic cyanobacteria, sulphate-reducing bacteria and other microbial consortia — can drive rapid carbonate accretion and generate microbialite fabrics controlled by local biogeochemical cycling, photosynthetically driven pH oscillations (Riding, 2000; Sun et al., 2016), and decaying organic matter (Sprachta et al., 2001). The draping laminae and inferred presence of extracellular mucilage at VdP are therefore consistent with sediment-stabilising microbial biofilms capable of rapid regeneration under high sediment-supply and burial rates. As also

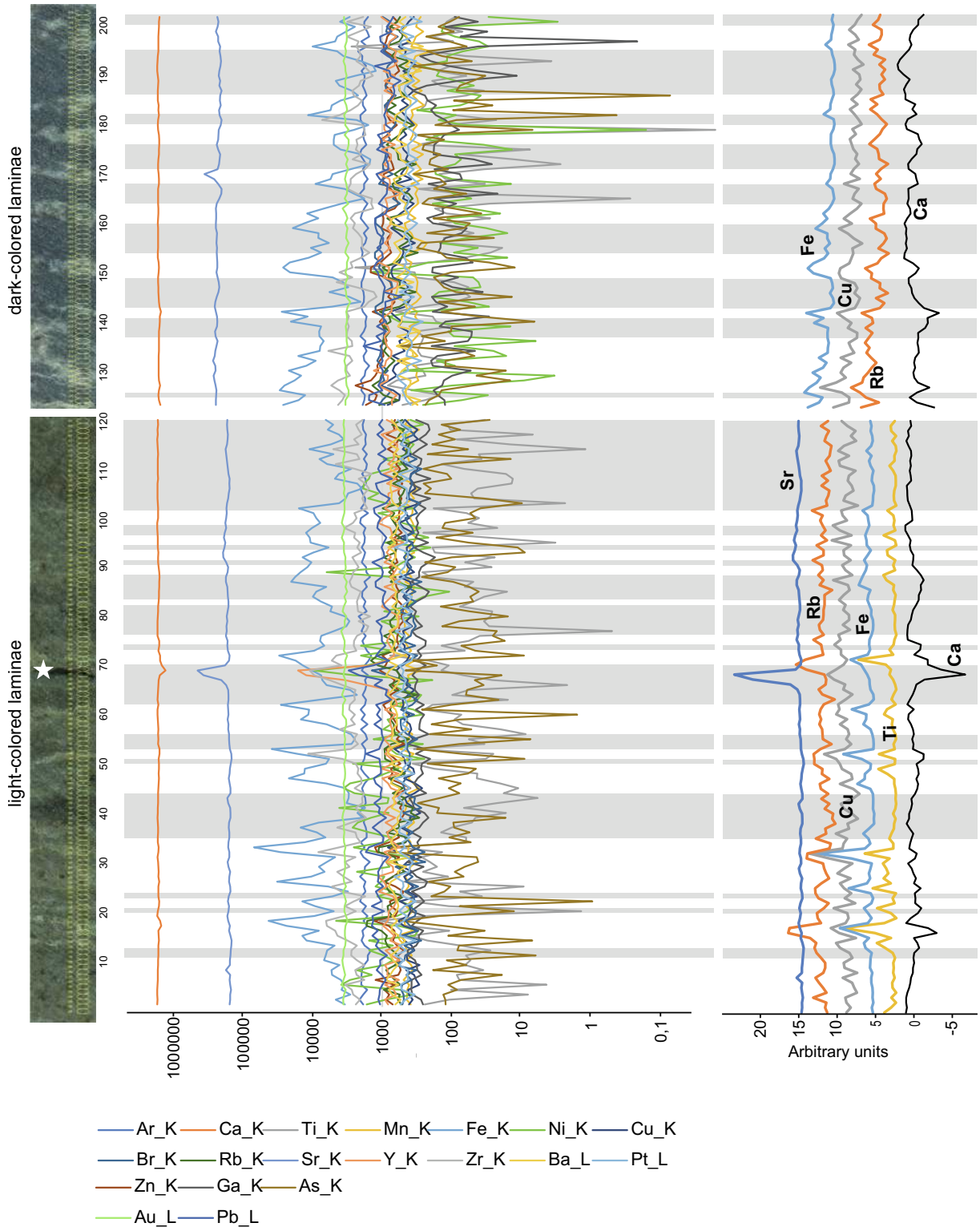

Fig. 6. Synchrotron Micro-XRF/XRD Elemental Maps & Patterns (Micro-Lamina scale). Detailed elemental heatmaps or line scan plots for key elements (e.g., Ar, Ca, Ti, Mn, Fe, Ni, Cu, Zn, Ga As, Br, Rb, Sr, Y, Zr, Ba, Pt, Au, Pb)) across representative dark/light micro-couplets (from A1, B1 thin sections). White star indicate an undetermined bone fragment preserved within laminae. Data are also reported in Table 1.

suggested by the taphonomy of the arthropods (Muscioni et al., 2025a), the entire rhythmite succession at VdP was likely deposited under strong microbial influence, a key factor enabling the exceptional preservation of fossil remains. Importantly, we find no geochemical or sedimentary evidence for sustained anoxic conditions; preservation is therefore best explained by rapid burial and microbial sealing under predominantly dysoxic–well oxygenated bottom waters rather than longlived euxinia.

The three nearly complete *Tethyshadros insularis* individuals recovered from VdP (MCSNT 57021, 57247, 57026) measure ~4–6 m in length, with estimated masses of ~400–600 kg and thoracic widths of ~60 cm (Chiarenza et al., 2021), comparable to large modern ungulates commonly used as taphonomic analogues. All three specimens display

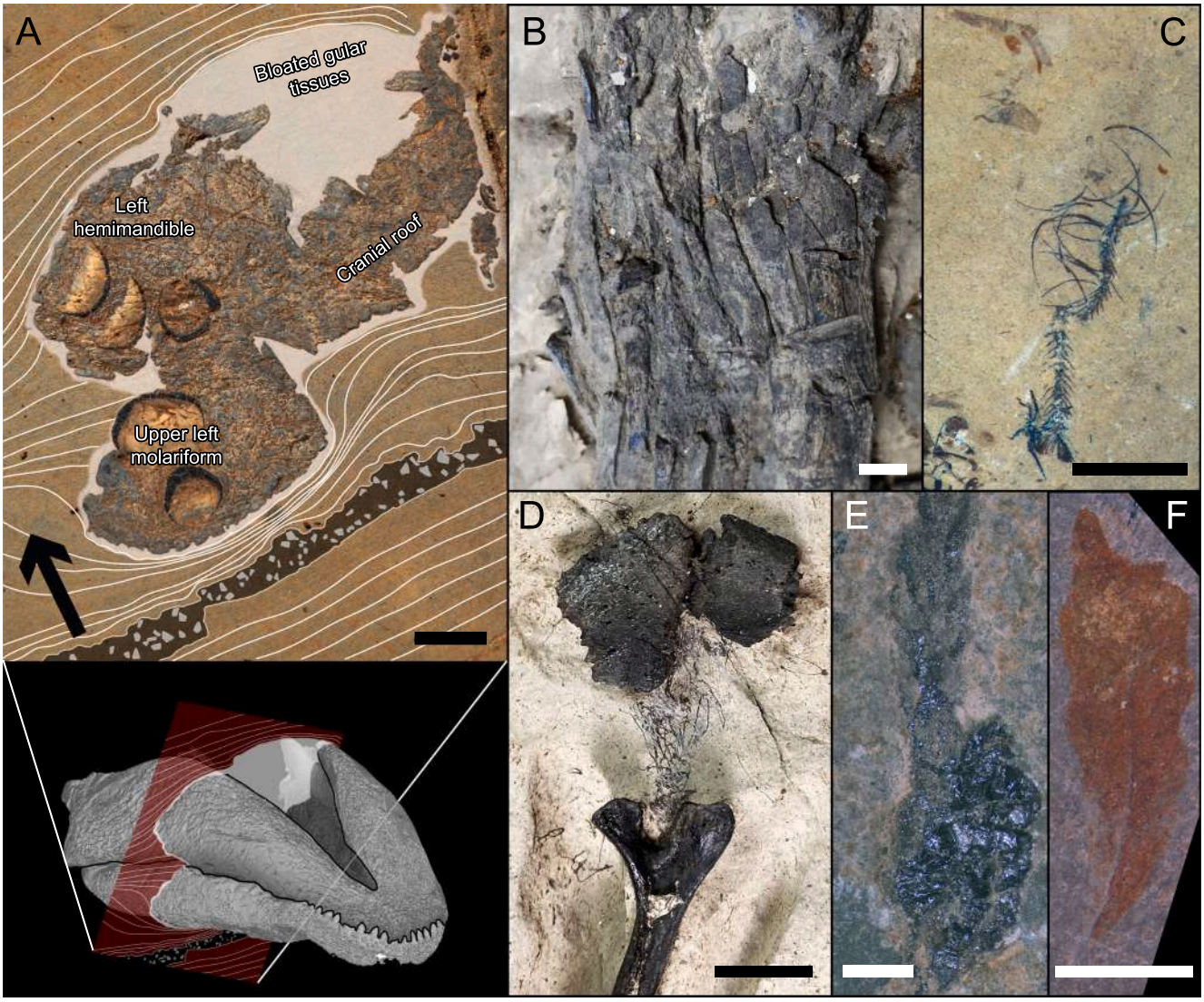

Fig. 7. Taphonomic modes and preservation styles at VdP. (A) burial dynamics of an *Acynodon adriaticus* skull (in situ section, top; 3D reconstruction, bottom). The specimen impacts the substrate post-flood deposition; onlapping laminae record the persistence of soft tissues during burial. (B) *Tethyshadros insularis* limb bone (MCSNT 57026) displaying longitudinal splitting consistent with subaerial exposure and desiccation. (C) Biotic interaction on slab MCSNT 15/21: decapod exuviae associated with a scavenged teleost carcass. (D) Disarticulated *A. adriaticus* remains (MCSNT 21.S239–1.0.22); associated carbonaceous filaments are interpreted as collagen fibres resulting from carcass maceration in the water column. (E) Compressed *Pagiophyllum*-like branch (MCSNT 57259); preservation quality implies rapid, parautochthonous burial. (F) Oxidised angiosperm leaf trace (MCSNT 15/18) indicative of prolonged transport from the hinterland. Scale bars: 10 mm (a–d), 5 mm (e, f).

passive postures — arched vertebral columns, asymmetrical limb positions and opisthotonic cervical curvature — consistent with post-mortem relaxation of submerged carcasses rather than peri-mortem convulsions (Weigelt, 1989; Reisdorf and Wuttke, 2012; Heinroth, 1923). Prior to acid-preparation, the holotype (MCSNT 57021) had near-intact articulation and carbonaceous soft-tissue outlines. Approximately 11 sets of daily tidal laminae directly overlie the in-situ skull, and laminae adjacent to the skull show convolution. MCSNT 57026, a partially collected *T. insularis* comprising a complete skull and limb elements, displays pronounced asymmetric (left–right) desiccation cracking on the skull and cortical splitting on long bones — features not observed in other VdP vertebrates (Fig. 7). The articulation and soft-tissue preservation in MCSNT 57021 imply rapid burial that limited decomposition and disarticulation driven by putrefaction gases. Scenarios involving prolonged surface flotation are inconsistent with both the degree of articulation and the preservation of soft-tissue traces. Adipocere formation, which typically requires weeks to months under stable anoxic conditions, is improbable here (Hobischak and Anderson, 2002; Petrik et al., 2004; Syme and Salisbury, 2014). Experimental studies show that floating durations vary by taxon and environment and that extended flotation usually yields progressive disarticulation (Weigelt, 1989; Brand et al., 2003), while fish and crustaceans can skeletonise carcasses within weeks (Petrik et al., 2004; Teather, 1994; Stuart and Ueland, 2017). The abundant palaemonid shrimps at VdP and evidence that the site functioned as a nursery imply active scavenger communities that would normally promote rapid disassembly of exposed carcasses (Muscioni et al., 2025a). Controlled burial experiments on juvenile *Crocodylus* demonstrate that rapid entombment can preserve articulated skeletons with soft-tissue residues (Syme and Salisbury, 2014), consistent with the preservation seen in MCSNT 57021. Taken together, the most parsimonious explanation for the articulated, soft-tissue-bearing *Tethyshadros* specimens is near-immediate burial by tidally mediated sedimentation punctuated by episodic high-discharge events. The ~11 daily laminae overlying the holotype skull document burial on a timescale of days to weeks, while convoluted lamination adjacent to the skull is consistent with local deformation by

gas release from the buried carcass. In contrast, desiccation cracking and poorer preservation in MCSNT 57026 indicate subaerial exposure and drying prior to transport, and we interpret this specimen as an allochthonous carcass segment entrained from inland and emplaced within the tidal inlet during a high-discharge event.

The in-situ position of *Acynodon adriaticus* MCSNT 57248, 57031 and unrecovered in-situ specimen (Muscioni et al., 2024) (Fig. 7) indicates deposition on the substrate in a belly-up orientation, with the mandible closed, the neck slightly laterally curved and forelimbs passively splayed (Muscioni et al., 2023; Muscioni et al., 2024; Delfino et al., 2008). A

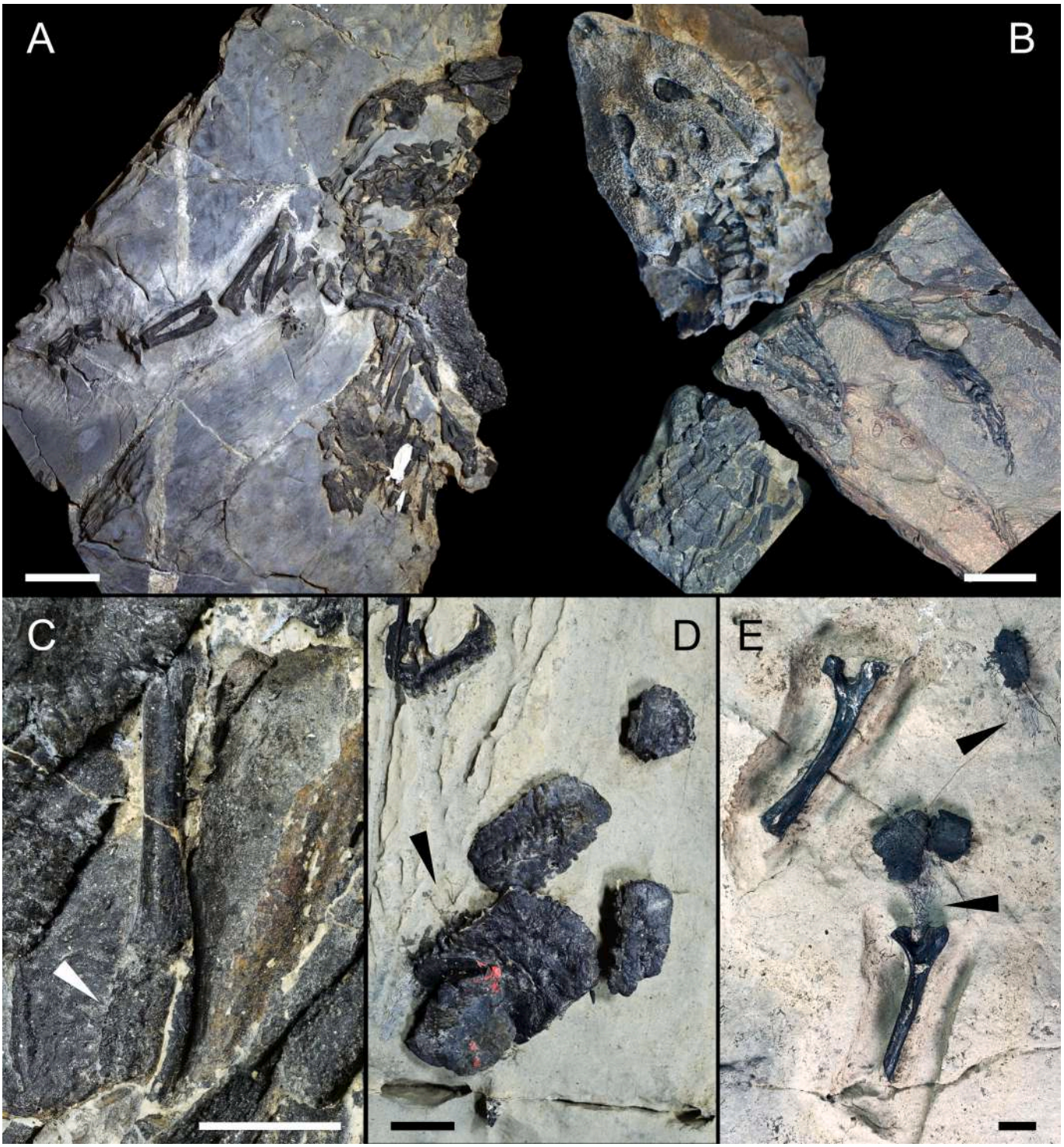

Fig. 8. Material assigned to *Acynodon adriaticus* with different preservations. (A) Articulated specimen MCSNT 57031, missing post-abdominal portion. (B) Articulated holotype and paratype MCSNT 57248, 57032, missing post-abdominal portions. (C) Detail of a dorsal rib from MCSNT 57032 showing different preservation of the rib (bone) and articulated proximal gastral element (highlighted with white arrow), here interpreted as more heavily altered and deformed due a cartilaginous/less mineralised original composition. (D, E) Clusters of associated osteoderms and dorsal ribs dropped from floating carcasses (MCSNT 21.S239–1.0.22). The original presence of macerated ligamentous tissues is manifested by carbonaceous filaments articulated to proximal portions of ribs and ventral surfaces of osteoderms (highlighted by black arrows). Scale bars: 50 mm (A, B), 10 mm (C-E).

second, currently undescribed crocodylomorph (MCSNT 24. S239–1.1205) is preserved in a similar supine posture. VdP preserves both isolated dispersed osteoderms and semi-articulated paravertebral shields in a shrunken/curled configuration (e.g., MCSNT 57031, 57032; MCSNT 21.S239 1.0.22). All articulated crocodilians lack posterior body portions; in several specimens (e.g., MCSNT 57031), the separation into anterior and posterior units is clear. Overlying laminae commonly form dome-like outlines between hemimandibles, and in MCSNT 57032 a volumetric trace of cartilagineous intermediate costal segment (sensu Escobar et al., 2025) is preserved articulated to the dorsal ribs. As with *Tethyshadros*, ~11 daily laminae occur above the in situ *Acynodon* skull (Figs. 7 and 8).

Carcasses lying on their backs are typically interpreted as the product of bloating by putrefaction gases in water, causing dorsal expansion and potential flotation (Weigelt, 1989; Syme and Salisbury, 2014) (Fig. 7). Semi-articulated paravertebral shields in a shrunken/curled state suggest partial leathery mummification, consistent with partial desiccation previously proposed to explain neck curvature in some specimens (Delfino et al., 2008). Weigelt's (Weigelt, 1989) observations of modern alligator carcasses indicate that differential emergence from water can produce both maceration and tissue mummification within days, so full desiccation is not required to explain such pattern. Experimental decay of small lepidosaurians (e.g., *Salvator merianae*) shows that bloating and abdominal liquefaction can cause anterior–posterior separation under weak surface turbulence and scavenger activity, after which the halves sink separately (Syme and Salisbury, 2014); similar splits are documented in fossil taxa (e.g., *Vadasaurus herzogi* AMNH FARB 32768 (Bever and Norell, 2017)). The size of the VdP crocodylians, only slightly larger than a tegu, makes comparable processes plausible. Carcasses that remained intact and floated would tend to disarticulate via maceration, producing dispersed ribs and osteoderms, whereas those that split lost buoyancy and settled with bloated soft tissues intact (Fig. 8). Dome-like laminae between hemimandibles and preserved costal cartilage indicate that burial occurred while soft tissues were still inflated. The ~11 daily laminae above the in situ *Acynodon* skull again indicate burial within days, sufficient to preserve bloated tissues and delicate soft-tissue structures.

Crocodilians, fish and crustaceans at VdP are generally preserved in relatively fresh condition. *Acynodon* specimens show limited post-mortem damage, and most fishes exhibit localised disarticulation

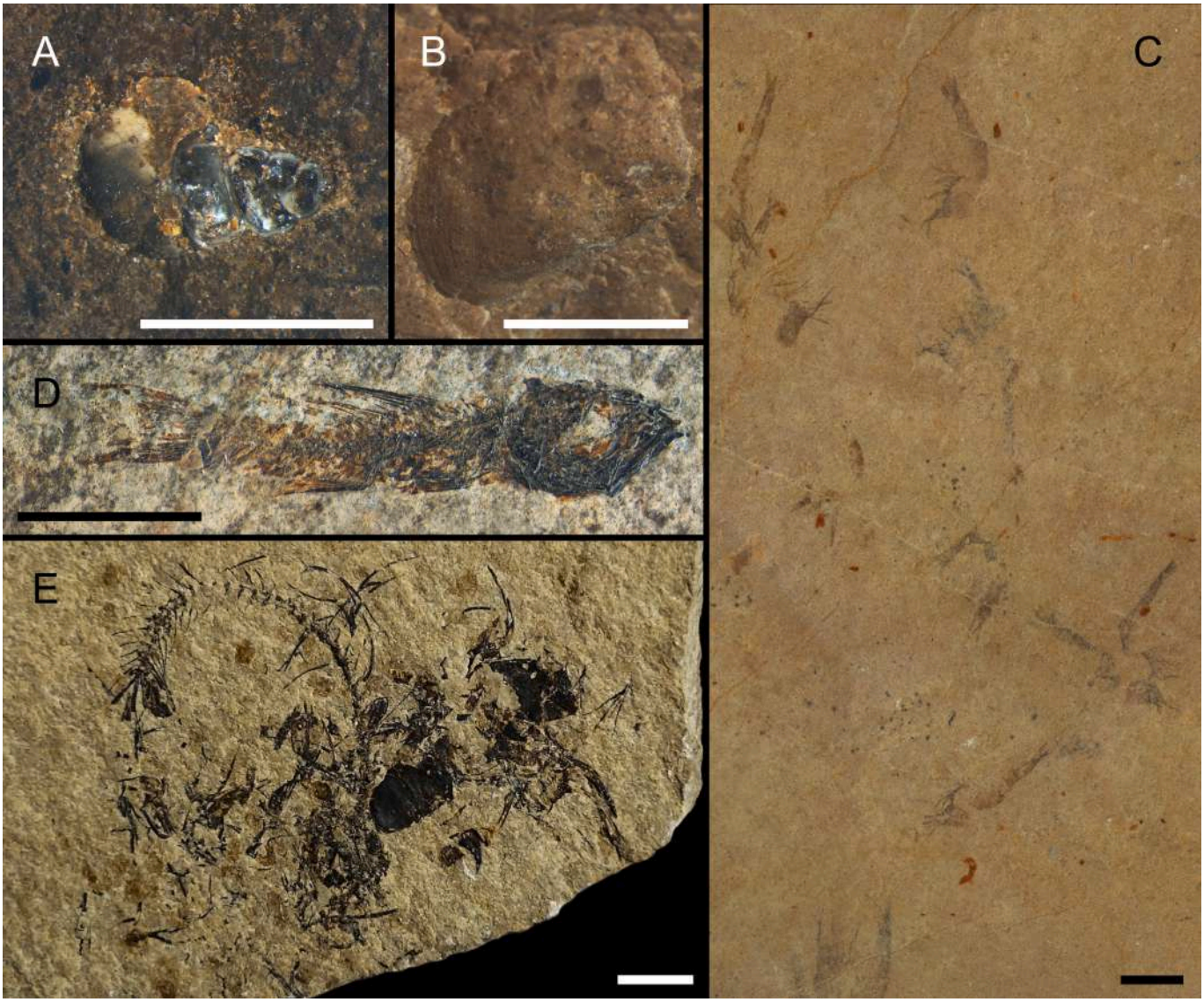

Fig. 9. Resident fauna of the Villaggio del Pescatore. (A) Gastropoda indet., MCSNT 57184. (B) Bivalvia indet., MCSNT 57232. (C) Decapod exuviae, MCSNT 10/51. (D) Fully articulated Teleostei indet. With soft tissues, MCSNT 23453. (E) Teleostei indet. MCSNT 15/86 exhibiting the typical ichtyofaunal taphonomy of the VdP (articulated spine and closely scattered paired and appendicular elements), likely due to arthropod scavenging. Scale bars: 5 mm.

patterns consistent with rapid arthropod scavenging after sinking rather than extensive transport or long-term exposure. Abundant decapods, together with nursery indicators, point to a resident arthropod community (Muscioni et al., 2025a; Fig. 9). *Tethyshadros* specimens show a broader range of taphonomic states: MCSNT 57021 is pristinely articulated with overlying laminae, MCSNT 57247 is associated with coarse debris and appears to have undergone more advanced decay, and MCSNT 57026 shows features indicative of prolonged subaerial exposure and dehydration. Isolated vertebrate elements, including a theropod metatarsal, a fragmentary *Doratodon* dentary and a pterosaur metacarpal, occur within the rhythmites (Chiarenza et al., 2021; Muscioni et al., 2025b; Dalla Vecchia, 2018). Filamentous carbonaceous residues on some bones are interpreted as degraded collagen or carbonised soft-tissue remnants (Figs. 7–8). The preservation state and ecological context of crocodylians, teleosts and decapods indicate that these taxa were resident components of the VdP tidal basin, buried within days to weeks of death. In contrast, the range of taphonomic alteration observed in *Tethyshadros* suggests mixed provenance: some individuals (e.g., MCSNT 57021) were entombed close to where they died, whereas others (e.g., MCSNT 57247, 57026) experienced subaerial exposure and limited transport before burial. Isolated bones of theropods, additional crocodylians and pterosaurs were likely washed into the basin from inland sources or derived from floating carcasses that disaggregated during maceration. Overall, the resident faunal assemblage is dominated by teleosts, crocodylians and arthropods (Fig. 9), whereas dinosaurs and some other vertebrates were supplied episodically from the surrounding catchment during high-discharge events.

The plant assemblage from the VdP rhythmites is largely allochthonous. Preservation and fragmentation range from poorly preserved compressions to exquisitely detailed impressions and mineralised tissue replacements, implying differing transport distances and histories (Figs. S1-S3). Some fragments with parallel, curved veins (e.g. MCSN 57259) resemble *Sabalites* leaf fragments described by Marmi et al. (Marmi et al., 2015; Fig. S3). *Sabalites* is known from coastal wetland lake margins in the lower Maastrichtian of Spain, where it is often associated with *Frenelopsis*, a genus also present in the VdP assemblage. Small, dispersed angiosperm and conifer leaves are also recorded (Fig. S2). In Cretaceous settings, small angiosperm leaves commonly characterise opportunistic taxa occupying fluctuating water levels and disturbed habitats (Marmi et al., 2015; Wang and Dilcher, 2018). The mixture of palm-like *Sabalites*, *Frenelopsis* and small angiosperm and conifer leaves at VdP indicates inputs from both coastal wetlands and the hinterland. Their preservation states and dispersal patterns are consistent with transport by storms and floods across a seasonally flooded coastal plain. This vegetational signal aligns with the vertebrate evidence for a dynamic, low-latitude, storm- and flood-prone coastal environment supplying both resident and allochthonous material to the tidal-flat depositional system.

4.4. *Palaeoclimate simulations and monsoon regime at Villaggio del Pescatore*

To test whether the Villaggio del Pescatore (VdP) tidal-flat system formed under a monsoon-dominated climate, we used palaeoclimate models (see Methods and SI) forced with alternative 85–80 Ma set palaeogeographies and CO_2 trajectories representative of greenhouse conditions (Scotese et al., 2025; Rae et al., 2021). Across this ensemble, we diagnosed monsoon domains with two complementary approaches: (i) the precipitation-seasonality criterion commonly used in modern monsoon assessments (Wang and Ding, 2008), and (ii) a Monsoon Precipitation Index (MPI) that captures subtler but strongly seasonal rainfall regimes. In all palaeoclimate experiments based on Scotese palaeogeographies (Scotese and Wright, 2018), the grid cells corresponding to the reconstructed position of the northern Adriatic Carbonate Platform (including the VdP area) fall within modelled monsoon domains (Figs. 10-S4). Using the Wang & Ding definition (Wang and Ding, 2008), the northern Tethyan margin at ~29°N is consistently flagged as monsoonal under both proxy-based CO_2 (after Rae et al. (Rae et al., 2021)) and a Scotese temperature–CO_2 curve configuration (Scotese et al., 2025), indicating a strong annual contrast between wet and dry seasons. MPI diagnostics corroborate this reconstruction, identifying the same region as monsoonal and classifying it as a summer-dominated system (blue MPI shading), with peak precipitation during the warm months (Figs. 10, S4). For example, modelled August precipitation fields from the high-resolution runs show a pronounced rainfall maximum (>10 mm/day) over the northern Tethyan margin at these latitudes, confirming that the diagnosed monsoon is not a purely 'dry' seasonal signal but reflects genuinely wet summers capable of driving frequent flood pulses. Sensitivity experiments exploring alternative early-middle Campanian palaeogeographies (i.e. simulating the palaeoclimatological effect of reconstructing no islands, small island archipelago or bigger emerged island landmasses) demonstrate that the strength and continuity of the monsoon belt are strongly modulated by the extent of emergent land around the Adriatic–Dinaric sector. In configurations with a more open Tethys and a highly fragmented island chain, the monsoon masks over the VdP region become patchier and weaker, and the MPI signal is more easily interrupted by adjacent oceanic cells. In contrast, Scotese reconstructions with a laterally extensive emergent Adriatic–Dinaric landmass produce a coherent monsoon domain and more spatially continuous summer rainfall maxima over the area that includes VdP. This behaviour is consistent with theoretical expectations that larger, contiguous landmasses enhance land–sea thermal contrast and intensify monsoon circulations relative to chains of small islands (Hurley and Boos, 2013; Ma et al., 2014; Mahmoud et al., 2021; Chen et al., 2025).

5. Monsoon enhanced tropical cyclones as a genetic control on the VdP Lagerstätte

Tropical cyclones (hurricanes/typhoons) and associated monsoon bursts are major agents of pulsed, high-magnitude sediment and freshwater delivery to modern tropical coasts (Wang et al., 2021; Clift and Jonell, 2021). At VdP, sedimentological, geochemical and taphonomic datasets collectively indicate that episodic, highenergy inputs exerted primary control on deposition and exceptional preservation. Coarse heterolithic clasts, matrix-supported breccia horizons incorporating reworked local clasts, cannibalised rhythmite pebbles, and centimetre-scale debris-flow beds match the expected signature of concentrated flood and overwash events (see SI a table summarizing carbonate facies at the VdP). Two principal transport modes are recorded in the succession: buoyant discharge plumes rich in terrestrial organic matter, supplying suspended fines and nutrients that settle over days to months and contribute to elevated TOC in dark lamina packages (Allison, 1988); and episodic hyperpycnal and overwash-style flows that deliver coarse clastic pulses, matrix-supported clasts/pebbles and transported megafauna onto the tidal flat (Allison and Briggs, 1993; Fig. 11). These event beds show clear terrigenous geochemical fingerprints (elevated Zr/Al_2O_3 and Ti/Al_2O_3 and positive $SiO_2(ex)$–Al_2O_3 covariation), while Sr/Ca and Ba(ex) peaks and higher TOC in darker packages mark intervals of enhanced productivity and variable salinity synchronous with these pulses (Figs. 5–6; Section 4.2).

The tidal physical template controlled how event pulses were archived. Alternation of fine, regularly laminated tidal couplets with centimetre-scale debris beds parallels modern tidal-flat successions, in which storm or flood beds interrupt otherwise continuous tidal lamination. Semidiurnal tidal forcing with neap–spring modulation, low-angle palaeotopography and the significant control exerted by tidal channels would have exerted strong control on sediment trapping: discharge during rising spring tides and transgression favours landward penetration and deposition, whereas discharge during ebb favours export. At VdP, consistent couplet thicknesses, systematic microslumping and neap–spring groupings all indicate rapid accumulation

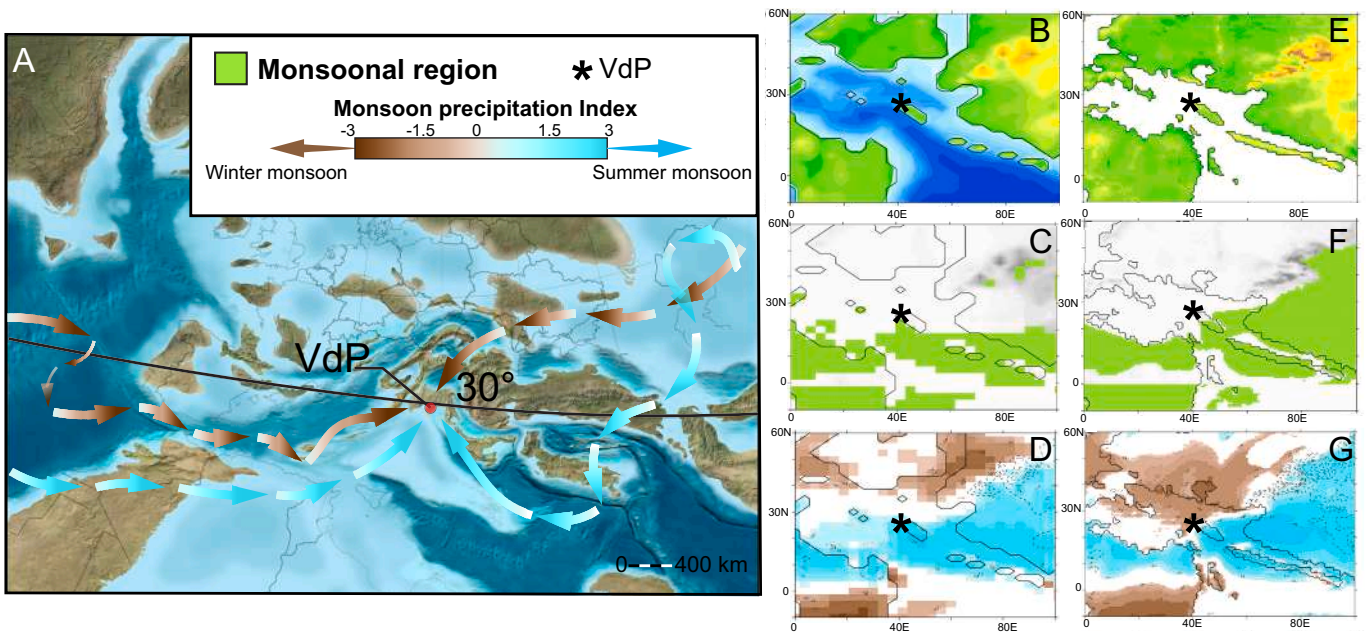

Fig. 10. Upper Cretaceous palaeogeography and simulated monsoon hydroclimate at the VdP locality. (A) Palaeogeographic reconstruction showing the position of the study area (VdP; red marker) at ~29° palaeolatitude and the inferred seasonal monsoon flow paths (brown arrows: winter monsoon; blue arrows: summer monsoon). Spatial patterns for the monsoonal season on palaeogeography with (B-D) low resolution and (*E*-G) high resolution palaeogeography; Palaeogeographic boundary conditions for GCM in B and E; C, F diagnosed monsoonal region (green); and D, G monsoon precipitation index (MPI; colour scale), where brown tones indicate stronger summer-monsoon dominance and blue tones indicate stronger winter-monsoon dominance. The VdP position is indicated by the star in all map panels. (For interpretation of the references to colour in this figure legend, the reader is referred to the web version of this article.)

on very low to flat relief slopes, with tides amplifying the trapping efficiency of storm-derived sediment pulses (Fig. 11). These rapid inputs occurred in a carbonate-saturated, microbially active sedimentary regime conducive to preservation. Microbial mats and extracellular mucilage stabilised freshly deposited sediment and promoted early cementation, reducing oxidation and bioturbation between events (Noffke et al., 2001; Peñalver et al., 2002; Iniesto et al., 2021; Marugán-Lobón et al., 2023; Dias and Carvalho, 2022; Muscioni et al., 2025a). The association of carbonaceous soft-tissue outlines on articulated crocodylians and hadrosauroids, fine lamination, TOC peaks and microbial fabrics fits a three-step sequence: (a) a flood or tropical-cyclone event delivers carcasses, plant debris and suspended fines onto the tidal flat; (b) rapid tidal drape buries this material and microbial colonisation generates a stabilising biofilm and carbonate crust; and (c) microbial stabilization, together with intermitted bottom-water stratification, limit bioturbation and promotes preservation of soft tissues and articulation (Fig. 11).

At the larger stratigraphic scale, the karstified basal contact, overlying epikarstic breccia and laterally confined lens of finely laminated rhythmites interbedded with carbonate pebbles are consistent with deposition during a transgressive pulse, as relative rising sea level increased accommodation and promoted landward facies migration (Armenteros et al., 1997; Mazzullo, 2006; Armenteros and Edwards, 2012; Platt and Wright, 2023). Within this transgressive framework, monsoon-enhanced tropical-cyclone and flash-flood pulses created highly effective preservation windows: increased accommodation reduced reworking, while tidal phasing focused and trapped successive event beds. Lamina chronometry (see Section 4.2) constrains decadalscale stacking (≈40 yr for the preserved lens), within which multiple flood events were archived during a single transgressive episode (Fig. 12).

Palaeoclimate simulations provide an independent test. Hadley Centre climate-model experiments using alternative palaeogeographic reconstructions (including Scotese configurations) and proxy-based CO_2 trajectories consistently diagnose monsoon regimes over the northern Tethyan margin at ~30°N, where the Adriatic Carbonate Platform (AdCP) and VdP were located. Palaeoclimate reconstructions (Fig. 10-S4) show that the VdP region falls within a summer-dominated monsoon belt, with strongly seasonal rainfall and pronounced wet summers. High-resolution precipitation fields from these simulations show rainfall maxima centred over the northern Adriatic–Dinaric sector, indicating that the modelled monsoon is not merely a dry seasonal cycle but a genuinely wet regime capable of sustaining frequent, high-magnitude flood pulses.

Sensitivity experiments show that monsoon strength and coherence are strongly modulated by emergent land extent in the Adriatic–Dinaric sector. Configurations with a more open Tethys and highly fragmented island chains, monsoon masks and MPI signals over the VdP area become patchier and weaker. By contrast, reconstructions with a laterally extensive emergent landmass produce a coherent monsoon domain and more spatially continuous summer rainfall over the northern AdCP. This behaviour is consistent with climatological theory in modern-monsoonal settings: larger contiguous land areas enhance land–sea thermal contrasts and intensify monsoon circulations relative to archipelagic settings. Consequently, the modelling supports palaeogeographic reconstructions in which VdP occupied the margin of a substantive emergent landmass rather than an isolated micro-island (Chiarenza et al., 2021), lending independent support to a continental margin depositional setting. The simulated hydroclimate pattern also mirrors the independent sedimentological, geochemical and palaeobotanical evidence from VdP. Modelled monsoon regimes at ~30°N imply humid summers and drier winters, matching the alternation between darker, TOC-rich lamina packages and lighter, better-ventilated intervals. Enhanced summer precipitation and runoff in the simulations provide a physically consistent driver for the high-magnitude flood pulses recorded by debris-flow and breccia beds, the terrigenous and nutrient pulses inferred from trace-element proxies and Ba(ex)/Sr/CaO trends, and the delivery of allochthonous plant material from a

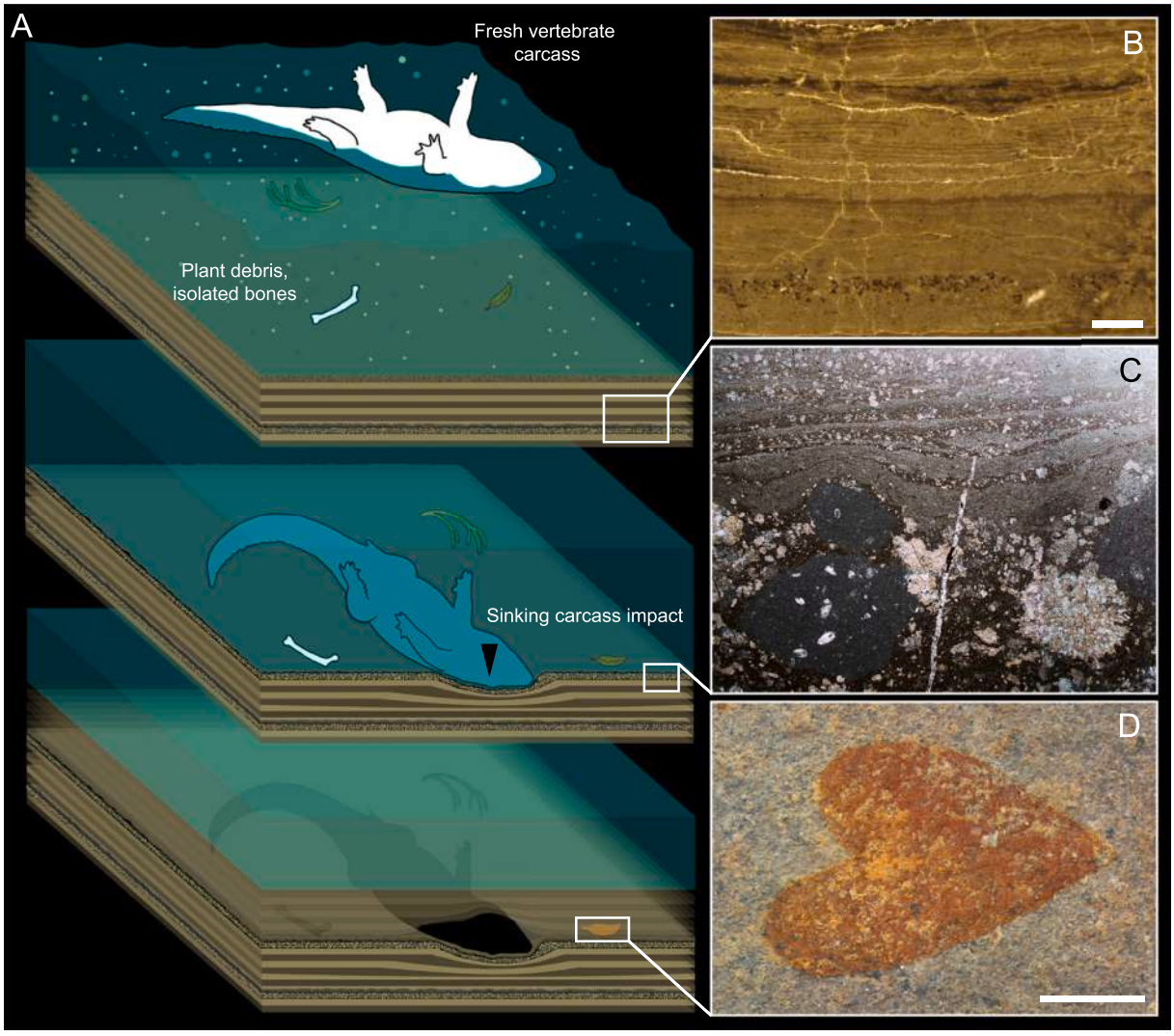

Fig. 11. Depositional model and facies details of the VdP deposits. (A) Reconstructed sequence of events: (Top) High-energy cyclonic events transport terrigenous debris, plant matter, and tetrapod carcasses across undisturbed tidal flats. (Middle) Coarse sediment settles to form a storm layer, rapidly stabilised by microbial mat draping; sinking vertebrate carcasses create impact deformation structures in the soft substrate. (Bottom) Resumption of tidal rhythms immediately buries isolated bones and debris, while articulated carcasses retain soft tissue, progressively buried by onlapping laminae over multiple tidal cycles. (B) Photomicrograph showing the typical fine, undisturbed rhythmic couplets. (C) A photographic detail illustrating an event bed, overlain by distinctive microbial draping structures. (D) A reddish, oxidised plant leaf transported from the hinterland, representing material delivered by flood pulses. Scale bars: 1 mm.

seasonally flooded coastal plain. Conversely, reduced monsoon activity corresponds to lighter, finer-grained lamina packages recording relatively drier conditions and improved bottom-water ventilation.

The composition and preservation of the VdP fossil assemblage are best explained by this model. Articulated small and large vertebrates, limited benthos and abundant palaemonid arthropods indicate selective preservation in a sheltered microenvironments repeatedly impacted by terrestrial flood plumes. Resident aquatic taxa (teleosts, crocodylians, crustaceans) appear to have been entombed near life position, whereas hadrosauroids display mixed taphonomic histories from in situ burial to limited transport. Coupled with modelling evidence for a coherent monsoondominated continental margin these patterns indicate that monsoon-enhanced tropical cyclones and flood regimes were a first-order control in producing the VdP, an potentially other, dinosaur *Konservat-Lagerstätte*.

6. Conclusions

Our multi-proxy investigation of the Villaggio del Pescatore (VdP) *Lagerstätte* establishes a coherent, event-driven mechanism for its formation. We demonstrate that this low-latitude Cretaceous site within the AdCP was a dynamic tidal flat, repeatedly impacted by monsoon-enhanced tropical-cyclone and flood events during a transgressive pulse. This climatic regime is consistent with VdP's ~ 29°N palaeolatitude, placing it near the Intertropical Convergence Zone where climate models predict pronounced summer wet seasons, strong seasonal moisture convergence, and recurrent tropical cyclone genesis under greenhouse conditions. We observe consistent trends at both the lamina-by-lamina and bulk-sample scales. High-resolution micro-XRF/XRD line scans across individual couplets show no new mineral phases between light and dark laminae, but instead reproducible shifts in relative abundance, including Ti, Ca, Rb, and Zr counts. These fine-scale patterns mirror package-scale signals measured on bulk powders: elevated Ti/Ca, Zr/Al, and Zr/Rb in darker, terrigenous-rich intervals; higher TOC and S in organic-rich packages; and Sr/Ca and Ba(ex) peaks, interpreted qualitatively as indicators of enhanced carbonate-producer input and nutrient pulses. Additional bulk indices, including Al_2O_3/K_2O and TiO_2/K_2O, track weathering/humidity shifts, while Zr/Rb and Ti/Ca act as grain-size and terrigenous-input proxies. Our proxy trends (runoff-linked terrigenous enrichments, productivity pulses, and

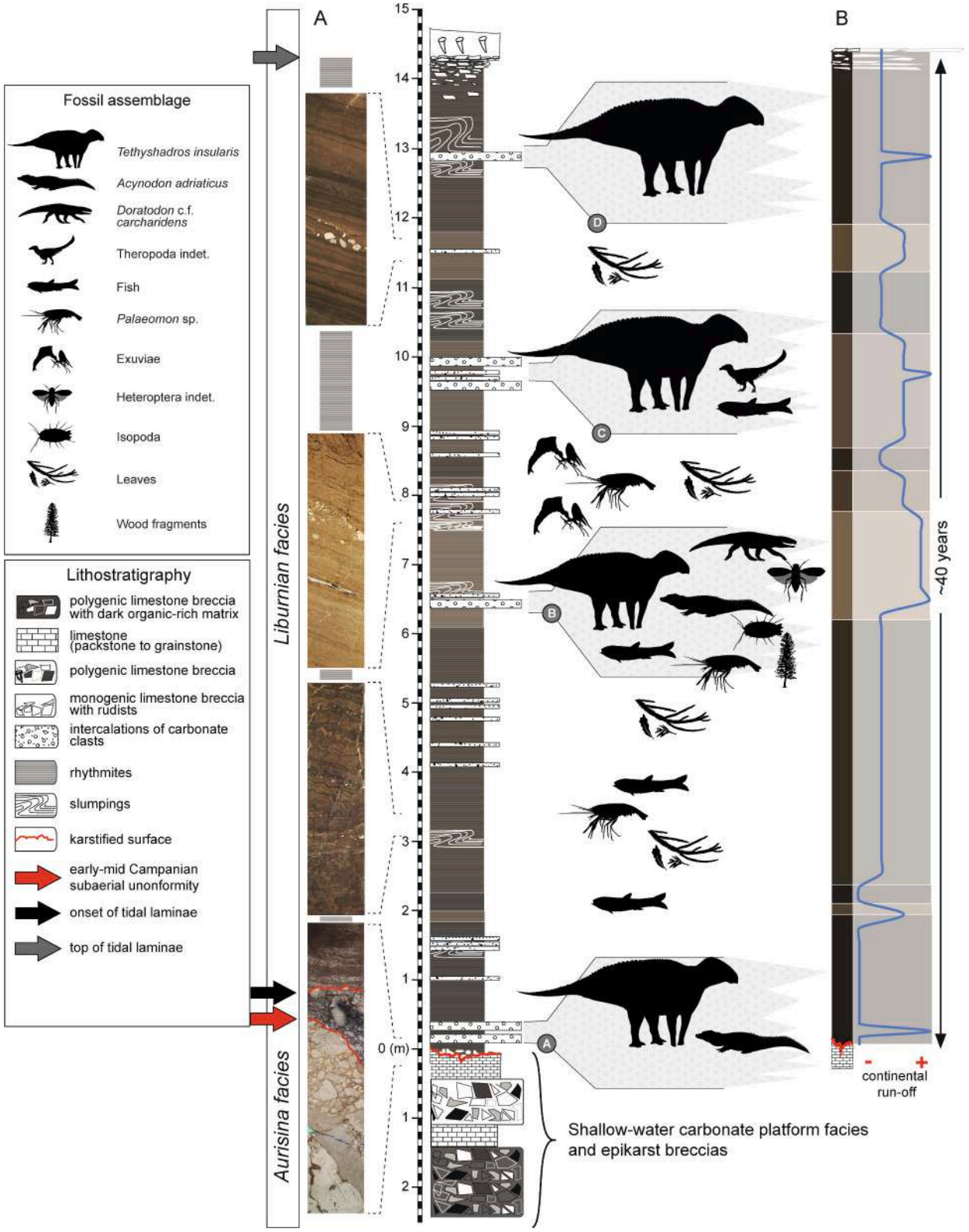

Fig. 12. Lithostratigraphy and occurrence of fossil remains at the VdP locality. Integration of outcrop data with Core S3 permits a high-resolution reconstruction of the Liburnian-like laminated facies. (A) Composite stratigraphic column of the exposed beds, coupled with detailed photographs from Core S3 showing the alternation of finely laminated carbonate rhythmites and interbedded debris-flow deposits. While plant, fish, and arthropod remains are ubiquitously distributed throughout the entire section, large vertebrate fossils (dinosaur and crocodylian remains) are explicitly restricted to specific stratigraphic intervals, marked as zones A–D, which are invariably associated with debris-flow deposits. (B) Schematic representation of inferred variations in continental runoff intensity over the ~40 year depositional interval of the VdP *Lagerstätte*, linking geochemical and sedimentological signals to phases of increased and reduced freshwater discharge.

alternating humid/drier signals) align with modelled expectations of greenhouse monsoon dynamics driven by strong land–sea thermal contrasts and warm sea-surface temperatures. This new genetic model for *Konservat-Lagerstätte* formation highlights how tidal processes set the baseline rhythm of sedimentation, efficiently trapping monsoon-driven supplies of terrigenous sediment, nutrients, carcasses, and plant debris. Crucially, microbial mats likely mediated rapid sealing and early diagenesis, preserving these inputs with exceptional fidelity, resulting in a decadal scale, daily resolved archive that uniquely records individual storm and flood events through coupled lithological, geochemical, palaeobotanical and taphonomic signatures. Together, these results indicate that extreme monsoon–tropical-cyclone regimes can generate decadal, daily-resolved windows of exceptional fossil preservation on carbonate tidal flats rather than merely restructuring coastal geomorphology. By linking tidal rhythmites, event beds, geochemical fingerprints, and taphonomy into a single process-based framework, VdP demonstrates how vertebrate *Konservat-Lagerstätten* can arise directly from the interaction of monsoon-enhanced flooding, tidal trapping, microbial sealing, and continental-scale land–sea thermal contrasts under greenhouse climates. We present the following testable criteria as a predictive template for identifying similar deposits in other low-latitude carbonate settings: (i) laterally continuous microcouplets (light–dark couplets) with micro-scale elemental maps showing no qualitatively distinct chemical end-members between laminae; (ii) intercalated event beds with matrix-supported clasts, erosive bases and debris-flow facies that locally host large vertebrates; (iii) stratigraphic alternation of terrigenous-enriched, high-TOC, S-rich intervals and finer, more oxygenated intervals revealed by bulk geochemical proxies (e.g., Ti/Ca, Zr/Rb, Sr/Ca, Ba(ex), Al_2O_3/K_2O); (iv) taphonomic evidence for rapid burial and microbial stabilization (e.g., draping laminae, soft-tissue outlines, early cementation fabrics); and (v) palaeoclimate model support for a monsoon-dominated precipitation regime at the palaeolatitude in question. Our mechanism therefore offers a predictive framework for locating and interpreting finely laminated, organic-rich successions in other low-latitude carbonate systems, and provides deep-time analogues for how intensifying monsoon–cyclone systems may alter sedimentation, ecosystem turnover and preservation potential along modern tropical coasts.

Author contributions (CRediT)

Conceptualization: FF, AAC.
Methodology: FF, AAC, AF.
Investigation: FF, CL. MM, LB, ED, MP, GB, AF, EK, SA, AAC.
Visualization: FF, MM, AF, AAC.
Funding acquisition: FF, AAC.
Project administration: FF, AAC.
Supervision: FF, AAC.
Writing – original draft: FF, AAC.
Writing – review & editing: FF, CL. MM, LB, ED, MP, GB, AF, EK, SA, AAC.

CRediT authorship contribution statement

Federico Fanti: Writing – review & editing, Writing – original draft, Visualization, Validation, Supervision, Software, Resources, Project administration, Methodology, Investigation, Funding acquisition, Formal analysis, Data curation, Conceptualization. **Lorenzo Consorti:** Writing – review & editing, Validation, Conceptualization. **Marco Muscioni:** Writing – review & editing, Visualization, Data curation. **Lorenzo Baldassari:** Methodology. **Enrico Dinelli:** Software, Resources, Investigation. **Maurizio Polentarutti:** Investigation. **Giorgio Bais:** Validation, Software, Conceptualization. **Alexander Farnsworth:** Visualization, Validation, Investigation, Formal analysis. **Evelyn Kustatscher:** Writing – review & editing, Validation, Investigation, Data curation. **Amalia Spina:** Validation, Investigation. **Alfio Alessandro Chiarenza:** Writing – review & editing, Writing – original draft, Visualization, Validation, Supervision, Software, Resources, Project administration, Methodology, Investigation, Funding acquisition, Formal analysis, Data curation, Conceptualization.

Declaration of competing interest

The authors declare that they have no known competing financial interests or personal relationships that could have appeared to influence the work reported in this paper.

Acknowledgements

This work culminates over four decades of sustained research since the discovery of the Villaggio del Pescatore site. We extend our profound gratitude to the numerous researchers, students, and enthusiastic collaborators whose dedicated time and invaluable resources have collectively contributed to unraveling the significance of this extraordinary locality. In particular, the scientific community is indebted to Mario Sartori di Borgoricco and Dr. Flavio Bacchia for their lifelong commitment to the site. We hope that these scientific findings underscore the uniqueness of this palaeontological site, fostering renewed commitment from all institutional bodies towards its protection and promotion.

We thank all those involved in the ongoing research project at VdP. Data and results presented in this study were made possible by the Accordo Quadro agreement between the Università di Bologna (Dip. BiGeA), Università di Trieste (Dip. MiGE), Museo Civico di Storia Naturale di Trieste, ISPRA, Elettra Sincrotrone, and ZOIC s.r.l. The Soprintendenza Archeologia, Belle Arti e Paesaggio del Friuli-Venezia Giulia (SABAP FVG) facilitated the study of fossil remains (prot. 3289 dd. 22 February 2022 to F.F.); we thank Dr.ssa P. Ventura, Dr.ssa F. Toffanin, Dr.ssa P. Loccardi, and Dr. R. Micheli for their commitment to scientific research at the site. Images reproduced by permission of the Soprintendenza ABAP FVG – MiC. Further reproduction of the images is regulated by current legislation (Art. 108, para. 3 of Legislative Decree 42/2004, as amended; Ministerial Decree 108 of 21/03/2024), and any further reproduction for profit is prohibited.

We are grateful to Dr.ssa P. Fasolato, Dr. F. Locci, and the staff of the Museo Civico di Storia Naturale di Trieste for granting access to material in their care, with special thanks to Dr.ssa D. Arbulla for her irreplaceable assistance. We also thank the Comune di Duino Aurisina for granting site access. We are indebted to Giorgia Bacchia, Tullio Perentin, and the entire ZOIC s.r.l. team for their professional preparation of fossil material, and to the staff of the TomoLab (Elettra Sincrotrone) for their hospitality and support. We acknowledge Elettra Sincrotrone Trieste for providing access to its synchrotron radiation facilities and we thank Alessandra Gianoncelli for the beamtime on the beamline TwinMic. Images of specimens are provided courtesy of Soprintendenza ABAP FVG-MiC (art. 108, co.3 D. Lgs 42/2004 s.m.i.).

Special thanks are given to Prof.ssa R. Capozzi, Prof. J. De Waele, and Prof. M. Antonellini (Dept. BiGeA, UniBo) for valuable comments and discussion that significantly improved this manuscript.

AAC is supported by The Royal Society – Newton International Fellowship (NIF\R1\231802). MM's PhD project is funded by the Next Generation EU: Piano Nazionale di Ripresa e Resilienza (PNRR) – XXXIX cycle (4184), STVA University of Bologna. AF also acknowledges the Leverhulme Grant (grant no. RPG-2019-365), NERC (grant NE/X013111/1) and the Chinese Academy of Sciences Visiting Professorship for Senior International Scientists (grant 2021FSE0001). AF acknowledges NERC grants NE/X015505/1 and NE/X018253/1.

Appendix A. Supplementary data

Supplementary data to this article can be found online at https://doi.org/10.1016/j.gloplacha.2026.105589.

Data availability

The authors confirm that all data necessary for supporting the scientific findings of this paper have been provided.

References

Allen, J., Spicer, R., Behrensmeyer, A., 1990. Transport hydrodynamics. In: Briggs and Crowther, pp. 227–235.

Allison, P.A., 1988. Konservat-Lagerstätten: cause and classification. Paleobiology 14, 331–344.

Allison, P.A., Briggs, D.E.G., 1993. Exceptional fossil record: distribution of soft-tissue preservation through the Phanerozoic. Geology 21, 527–530.

Ando, A., Kawahata, H., Kakegawa, T., 2006. Sr/Ca ratios as indicators of varying modes of pelagic carbonate diagenesis in the ooze, chalk and limestone realms. Sediment. Geol. 191, 37–53.

Arbulla, D., Cotza, F., Cucchi, F., Dalla Vecchia, F.M., De Giusto, A., Flora, O., Masetti, D., Palci, A., Pittau, P., Pugliese, N., Stenni, B., Tarlao, A., Tunis, G., Zini, L., 2006. La successione Santoniano–Campaniana del Villaggio del Pescatore (Carso Triestino) nel quale sono stati rinvenuti i resti di dinosauro. In: Guida alle Escursioni/Excursions Guide. Società Paleontologica Italiana EUT Edizioni Università di Trieste, Trieste, pp. 20–27.

Armenteros, I., Edwards, N., 2012. Palaeogeographic, palaeoclimatic, palaeohydrological and chemical/biochemical controls on accumulation of late Eocene coastal lacustrine–palustrine limestones, southern England. Sediment. Geol. 281, 101–118.

Armenteros, I., Daley, B., García, E., 1997. Lacustrine and palustrine facies in the Bembridge Limestone (late Eocene, Hampshire Basin) of the Isle of Wight, southern England. Palaeogeogr. Palaeoclimatol. Palaeoecol. 128, 111–132.

Bassetti, M.-A., Berné, S., Sicre, M.-A., Dennielou, B., Alonso, Y., Buscail, R., Jalali, B., Hebert, B., Menniti, C., 2016. Holocene hydrological changes in the Rhône River (NW Mediterranean) as recorded in the marine mud belt. Clim. Past 12, 1539–1553.

Bever, G.S., Norell, M.A., 2017. A new rhynchocephalian (Reptilia: Lepidosauria) from the late Jurassic of Solnhofen (Germany) and the origin of the marine Pleurosauridae. R. Soc. Open Sci. 4, 170570.

Brand, L., Hussey, M., Taylor, J., 2003. Decay and disarticulation of small vertebrates in controlled experiments. J. Taphon. 1.

Chen, L., Valdes, P.J., Farnsworth, A., 2025. The role of the North American continent in strengthening the Asian summer monsoon. Sci. Adv. 11, eadu8589.

Chiarenza, A.A., Fabbri, M., Consorti, L., Muscioni, M., Evans, D.C., Cantalapiedra, J.L., Fanti, F., 2021. An Italian dinosaur Lagerstätte reveals the tempo and mode of hadrosauriform body size evolution. Sci. Rep. 11, 23295.

Chiarenza, A.A., Mannion, P.D., Farnsworth, A., Carrano, M.T., Varela, S., 2022. Climatic constraints on the biogeographic history of Mesozoic dinosaurs. Curr. Biol. 32, 570–585 e3.

Chiarenza, A.A., Cantalapiedra, J.L., Jones, L.A., Gamboa, S., Galván, S., Farnsworth, A. J., Valdes, P.J., Sotelo, G., Varela, S., 2024. Early Jurassic origin of avian endothermy and thermophysiological diversity in dinosaurs. Curr. Biol. 34, 2517–2527 e4.

Clift, P.D., Jonell, T.N., 2021. Monsoon controls on sediment generation and transport: mass budget and provenance constraints from the Indus River catchment, delta and submarine fan over tectonic and multimillennial timescales. Earth Sci. Rev. 220, 103682.

Clift, P.D., Wan, S., Blusztajn, J., 2014. Reconstructing chemical weathering, physical erosion and monsoon intensity since 25 Ma in the northern South China Sea: a review of competing proxies. Earth Sci. Rev. 130, 86–102.

Consorti, L., Frijia, G., Caus, E., 2017. Rotaloidean foraminifera from the Upper cretaceous carbonates of Central and Southern Italy and their chronostratigraphic age. Cretac. Res. 70, 226–243.

Consorti, L., Arbulla, D., Bonini, L., Fabbi, S., Fanti, F., Franceschi, M., Frijia, G., Pini, G. A., 2021. The Mesozoic palaeoenvironmental richness of the Trieste Karst. GFT&M. https://doi.org/10.3301/GFT.2021.06.

Dalla Vecchia, F.M., 2009. Tethyshadros insularis, a new hadrosauroid dinosaur (Ornithischia) from the Upper cretaceous of Italy. J. Vertebr. Paleontol. 29, 1100–1116.

Dalla Vecchia, F.M., 2018. A wing metacarpal from Italy and its implications for latest cretaceous pterosaur diversity. Geol. Soc. Lond. Spec. Publ. 455, 209–219.

Dalla Vecchia, F.M., 2020. The Unusual Tail of Tethyshadros Insularis (Dinosauria, Hadrosauroidea) from the Adriatic Island of the European Archipelago, 46.

Debeljak, I., Košir, A., Buffetaut, E., Otoničar, B., 2002. The late cretaceous dinosaurs and crocodiles of Kozina (SW Slovenia): a preliminary study. Mem. Soc. Geol. Ital. 57, 193–201.

Delfino, M., Martin, J.E., Buffetaut, E., 2008. A new species of Acynodon (Crocodylia) from the Upper Cretaceous (Santonian–Campanian) of Villaggio del Pescatore, Italy. Palaeontology 51, 1091–1106.

Dias, J.J., Carvalho, I. de S., 2022. The role of microbial mats in the exquisite preservation of Aptian insect fossils from the Crato Lagerstätte, Brazil. Cretac. Res. 130, 105068.

Diedrich, C., Caldwell, M.W., Gingras, M., 2011. High-resolution stratigraphy and palaeoenvironments of the intertidal flats to lagoons of the Cenomanian (Upper cretaceous) of Hvar Island, Croatia, on the Adriatic Carbonate Platform. Carbonates Evaporites 26, 381–399.

Dubiel, R.F., Parrish, J.T., Parrish, J.M., Good, S.C., 1991. The Pangaean Megamonsoon: evidence from the Upper Triassic Chinle Formation, Colorado Plateau. PALAIOS 6, 347.

Engelke, J., Linnert, C., Niebuhr, B., Schnetger, B., Brumsack, H.-J., Mutterlose, J., Wilmsen, M., 2018. Tracking late cretaceous environmental change: Geochemical environment of the upper Campanian to lower Maastrichtian chalks at Kronsmoor, northern Germany. Cretac. Res. 84, 323–339.

Escobar, G.A., Zaracho, V.H., Monferran, M.D., Luna, C.A., Cuaranta, P., 2025. Comprehensive postcranial osteology of the black yacare, *Caiman yacare* (Alligatoridae: Caimaninae): detailed descriptions, illustrations, and comparison across Crocodylia. Zool. J. Linnean Soc. 205, zlaf168.

Farnsworth, A., Lunt, D.J., Robinson, S.A., Valdes, P.J., Roberts, W.H.G., Clift, P.D., Markwick, P., Su, T., Wrobel, N., Bragg, F., Kelland, S.-J., Pancost, R.D., 2019. Past East Asian monsoon evolution controlled by paleogeography, not CO2. Sci. Adv. 5, eaax1697.

Fornaciari, E., Giusberti, L., Luciani, V., Tateo, F., Agnini, C., Backman, J., Oddone, M., Rio, D., 2007. An expanded cretaceous–Tertiary transition in a pelagic setting of the Southern Alps (central-western Tethys). Palaeogeogr. Palaeoclimatol. Palaeoecol. 255, 98–131.

Freeman, A., Jose, F., Roberts, H., Stone, G., 2015. Storm induced hydrodynamics and sediment transport in a coastal Louisiana lake. Estuar. Coast. Shelf Sci. 161, 65–75.

Frijia, G., Parente, M., Di Lucia, M., Mutti, M., 2015. Carbon and strontium isotope stratigraphy of the Upper cretaceous (Cenomanian–Campanian) shallow-water carbonates of southern Italy: Chronostratigraphic calibration of larger foraminifera biostratigraphy. Cretac. Res. 53, 110–139.

Furgerot, L., Mouazé, D., Tessier, B., Perez, L., Haquin, S., Weill, P., Crave, A., 2016. Sediment transport induced by tidal bores: an estimation from suspended matter measurements in the Sée River (Mont-Saint-Michel Bay, northwestern France). Compt. Rendus Geosci. 348, 432–441.

Gischler, E., Gibson, M.A., Oschmann, W., 2008. Giant Holocene freshwater microbialites, Laguna Bacalar, Quintana Roo, Mexico. Sedimentology 55, 1293–1309.

Godet, A., Suarez, M.B., Price, D., Lehrmann, D.J., Adams, T., 2023. Paleoenvironmental constraints on shallow-marine carbonate production in central and West Texas during the Albian (early cretaceous). Cretac. Res. 144, 105462.

Grabowski, J., Stoykova, K., Wierzbowski, H., Wójcik-Tabol, P., 2021. Upper Berriasian chemostratigraphy, clay minerals and calcareous nannofossils of the Barlya section (Western Balkan, Bulgaria): Implications for palaeoclimate and productivity changes, and stratigraphic correlations across the Alpine Tethys. Palaeogeogr. Palaeoclimatol. Palaeoecol. 567, 110252.

Guerreiro, C.V., Ziveri, P., Cavaleiro, C., Stuut, J.-B.W., 2024. Coccolith-calcite Sr/ca as a proxy for transient export production related to Saharan dust deposition in the tropical North Atlantic. Sci. Rep. 14, 4295.

Heinroth, O., 1923. Die Flügel von Archaeopteryx. J. Ornithol. 71, 277–283.

Hetzel, A., März, C., Vogt, C., Brumsack, H.-J., 2011. Geochemical environment of Cenomanian–Turonian black shale deposition at Wunstorf (northern Germany). Cretac. Res. 32, 480–494.

Hobischak, N., Anderson, G., 2002. Time of submergence using aquatic invertebrate succession and decompositional changes. J. Forensic Sci. 47, 142–151.

Hurley, J.V., Boos, W.R., 2013. Interannual variability of monsoon precipitation and local subcloud equivalent potential temperature. J. Clim. 26, 9507–9527.

Iniesto, M., Gutiérrez-Silva, P., Dias, J.J., Carvalho, I.S., Buscalioni, A.D., López-Archilla, A.I., 2021. Soft tissue histology of insect larvae decayed in laboratory experiments using microbial mats: Taphonomic comparison with cretaceous fossil insects from the exceptionally preserved biota of Araripe, Brazil. Palaeogeogr. Palaeoclimatol. Palaeoecol. 564, 110156.

Jurkovšek, B., Biolchi, S., Furlani, S., Kolar-Jurkovšek, T., Zini, L., Jež, J., Cucchi, F., 2016. Geology of the Classical Karst Region (SW Slovenia–NE Italy). J. Maps 12 (sup1), 352–362. https://doi.org/10.1080/17445647.2016.1215941.

Kimmig, J., Schiffbauer, J.D., 2024. A modern definition of Fossil-Lagerstätten. Trends Ecol. Evol. 39, 621–624.

Křížová, B., Consorti, L., Cardelli, S., Schmitt, K.E., Brombin, V., Franceschi, M., Tunis, G., Bonini, L., Frijia, G., 2024. Late cretaceous (Cenomanian–Turonian) temperature evolution and biotic response in the Adriatic Carbonate Platform region of Friuli, Northeast Italy. Palaeogeogr. Palaeoclimatol. Palaeoecol. 637, 111995.

Kuecher, G.J., Woodland, B.G., Broadhurst, F.M., 1990. Evidence of deposition from individual tides and of tidal cycles from the Francis Creek Shale (host rock to the Mazon Creek Biota), Westphalian D (Pennsylvanian), northeastern Illinois. Sediment. Geol. 68, 211–221.

Kvale, E.P., Cutright, J., Bilodeau, D., Archer, A., Johnson, H.R., Pickett, B., 1995. Analysis of modern tides and implications for ancient tidalites. Cont. Shelf Res. 15, 1921–1943.

Lodowski, D.G., Grabowski, J., 2023. Tracing the latest Jurassic–earliest cretaceous paleoenvironment evolution in swell carbonate facies: a case study of the High-Tatric succession (Central Western Carpathians, Tatra Mts, Poland). Acta Geol. Pol. 73, 741–772.

Ma, D., Boos, W., Kuang, Z., 2014. Effects of orography and surface heat fluxes on the south Asian summer monsoon. J. Clim. 27, 6647–6659.

Mahmoud, M.T., Mohammed, S.A., Hamouda, M.A., Mohamed, M.M., 2021. Impact of topography and rainfall intensity on the accuracy of IMERG precipitation estimates in an arid region. Remote Sens. 13, 13.

Marmi, J., Martín-Closas, C., Fernández-Marrón, M.T., Fondevilla, V., Gomez, B., 2015. A riparian plant community from the upper Maastrichtian of the Pyrenees (Catalonia, NE Spain). Cretac. Res. 56, 510–529.

Marugán-Lobón, J., Martín-Abad, H., Buscalioni, Á.D., 2023. The Las Hoyas Lagerstätte: a palaeontological view of an early Cretaceous wetland. J. Geol. Soc. Lond. 180, jgs2022-079.
Mazzullo, S.J., 2006. Late Pliocene to Holocene platform evolution in northern Belize, and comparison with coeval deposits in southern Belize and the Bahamas. Sedimentology 53, 1015–1047.
Mitchell, A.J., Uličný, D., Hampson, G.J., Allison, P.A., Gorman, G.J., Piggott, M.D., Wells, M.R., Pain, C.C., 2010. Modelling tidal current-induced bed shear stress and palaeocirculation in an epicontinental seaway: the Bohemian Cretaceous Basin, Central Europe. Sedimentology 57, 359–388.
Muscente, A.D., Schiffbauer, J.D., Broce, J., Laflamme, M., O'Donnell, K., Boag, T.H., Meyer, M., Hawkins, A.D., Huntley, J.W., McNamara, M., MacKenzie, L.A., Stanley Jr., G.D., Hinman, N.W., Hofmann, M.H., Xiao, S., 2017. Exceptionally preserved fossil assemblages through geologic time and space. Gondwana Res. 48, 164–188.
Muscioni, M., Chiarenza, A.A., Delfino, M., Fabbri, M., Milocco, K., Fanti, F., 2023. Acynodon adriaticus from Villaggio del Pescatore (Campanian of Italy): Anatomical and chronostratigraphic integration improves phylogenetic resolution in Hylaeochampsidae (Eusuchia). Cretac. Res. 151, 105631.
Muscioni, M., Chiarenza, A.A., Fernandez, D.B.H., Dreossi, D., Bacchia, F., Fanti, F., 2024. Cranial anatomy of Acynodon adriaticus and extreme durophagous adaptations in Eusuchia (Reptilia: Crocodylomorpha). Anat. Rec. 307, 3653–3684.
Muscioni, M., Chiarenza, A.A., Nicholl, C.S.C., Perentin, T., Dreossi, D., Fanti, F., 2025a. A ziphodont crocodylomorph from Villaggio del Pescatore Lagerstätte (Campanian, Italy). Zool. J. Linnean Soc. 205, zlaf171.
Muscioni, M., Garassino, A., Colla, A., Bruce, N., Chiarenza, A.A., Fanti, F., 2025b. An Upper Cretaceous arthropod assemblage from Villaggio del Pescatore (Campanian, Italy) and its implications for peri-Tethyan palaeobiogeography and palaeoecology. Pap. Palaeontol. 11, e70048.
Noffke, N., Gerdes, G., Klenke, T., Krumbein, W.E., 2001. Microbially induced sedimentary structures: a new category within the classification of primary sedimentary structures. J. Sediment. Res. 71, 649–656.
Noto, C., 2010. Hierarchical control of terrestrial vertebrate taphonomy over space and time: discussion of mechanisms and implications for vertebrate paleobiology, 32, 287–336.
O'Brien, C.L., Robinson, S.A., Pancost, R.D., Sinninghe Damsté, J.S., Schouten, S., Lunt, D.J., Alsenz, H., Bornemann, A., Bottini, C., Brassell, S.C., Farnsworth, A., Forster, A., Huber, B.T., Inglis, G.N., Jenkyns, H.C., Linnert, C., Littler, K., Markwick, P., McAnena, A., Mutterlose, J., Naafs, B.D.A., Püttmann, W., Sluijs, A., van Helmond, N.A.G.M., Vellekoop, J., Wagner, T., Wrobel, N.E., 2017. Cretaceous sea-surface temperature evolution: Constraints from TEX86 and planktonic foraminiferal oxygen isotopes. Earth Sci. Rev. 172, 224–247.
Palci, A., 2003. Ricostruzione Paleoambientale del Sito Fossilifero Senoniano del Villaggio del Pescatore (Trieste). Thesis. Università degli Studi di Trieste, Trieste.
Paytan, A., Griffith, E.M., 2007. Marine barite: Recorder of variations in ocean export productivity. Deep-Sea Res. II Top. Stud. Oceanogr. 54, 687–705.
Peñalver, E., Delclòs, X., De Renzi, M., 2002. Evidence of continental microbial mats based on the study of fossil insects: examples from two Spanish Konservat Fossil-Lagerstätten, pp. 281–287.
Petrik, M.S., Hobischak, N.R., Anderson, G.S., 2004. Examination of factors surrounding human decomposition in freshwater: a review of body recoveries and coroner cases in British Columbia. J. Can. Soc. Forensic Sci. 37, 9–17.
Platt, N.H., Wright, V.P., 2023. Flooding of a carbonate platform: the Sian Ka'an Wetlands, Yucatán, Mexico—a model for the formation and evolution of palustrine carbonate factories around the modern Caribbean Sea and in the depositional record. Depositional Rec. 9, 99–151.
Rae, J.W.B., Zhang, Y.G., Liu, X., Foster, G.L., Stoll, H.M., Whiteford, R.D.M., 2021. Atmospheric CO2 over the past 66 million years from marine archives. Annu. Rev. Earth Planet. Sci. 49, 609–641.
Reisdorf, A.G., Wuttke, M., 2012. Re-evaluating Moodie's opisthotonic-posture hypothesis in fossil vertebrates part I: Reptiles—the taphonomy of the bipedal dinosaurs Compsognathus longipes and Juravenator starki from the Solnhofen Archipelago (Jurassic, Germany). Palaeobiodivers. Palaeoenviron. 92, 119–168.
Rejmánek, M., Sasser, C.E., Peterson, G.W., 1988. Hurricane-induced sediment deposition in a gulf coast marsh. Estuar. Coast. Shelf Sci. 27, 217–222.
Retallack, G.J., 1990a. A long-term natural experiment in pedogenesis. In: Retallack, G.J. (Ed.), Soils of the Past: An Introduction to Paleopedology. Springer Netherlands, Dordrecht, pp. 291–294.
Retallack, G.J., 1990b. Alteration of paleosols after burial. In: Retallack, G.J. (Ed.), Soils of the Past: An Introduction to Paleopedology. Springer Netherlands, Dordrecht, pp. 129–145.
Riding, R., 2000. Microbial carbonates: the geological record of calcified bacterial–algal mats and biofilms. Sedimentology 47, 179–214.
Rosas, A., García-Tabernero, A., Fidalgo, D., Fero Meñe, M., Ebana Ebana, C., Esono Mba, F., Morales, J.I., Saladie, P., 2022. The scarcity of fossils in the African rainforest: archaeo-paleontological surveys and actualistic taphonomy in Equatorial Guinea. Hist. Biol. 34, 1582–1590.
Rosatelli, G., Castorina, F., Consalvo, A., Brozzetti, F., Ciavardelli, D., Perna, M.G., Bell, K., Bello, S., Stoppa, F., 2023. Elemental abundances and isotopic composition of Italian limestones: Glimpses into the evolution of the Tethys. J. Asian Earth Sci. X 9, 100136.
Schimmelmann, A., Lange, C.B., Schieber, J., Francus, P., Ojala, A.E.K., Zolitschka, B., 2016. Varves in marine sediments: a review. Earth Sci. Rev. 159, 215–246.
Scotese, C.R., 2021. An Atlas of Phanerozoic Paleogeographic Maps: the seas come in and the seas go out. Annu. Rev. Earth Planet. Sci. 49, 679–728.
Scotese, C., Wright, N., 2018. PaleoDEM Resource – Scotese and Wright (2018) – EarthByte. https://www.earthbyte.org/paleodem-resource-scotese-and-wright-2018/.
Scotese, C.R., Vérard, C., Burgener, L., Elling, R.P., Kocsis, A.T., 2025. The Cretaceous world: plate tectonics, palaeogeography and palaeoclimate. Geol. Soc. Lond. Spec. Publ. 544, SP544-2024-28.
Spalluto, L., Petruzzelli, M., Sabato, L., Tropeano, M., 2025. Cretaceous cyclic peritidal carbonates of the Apulia Carbonate Platform (Apulia, southern Italy) in a hierarchical sequence-stratigraphic perspective: a case study from the Murge area (the Giovinazzo Sea-cliff section). Depositional Rec. 11, 328–353.
Sprachta, S., Camoin, G., Golubic, S., Le Campion, Th., 2001. Microbialites in a modern lagoonal environment: nature and distribution, Tikehau atoll (French Polynesia). Palaeogeogr. Palaeoclimatol. Palaeoecol. 175, 103–124.
Steel, R.J., Plink-Bjorklund, P., Aschoff, J., 2012. Tidal deposits of the Campanian Western Interior Seaway, Wyoming, Utah and Colorado, USA. In: Davis Jr., R.A., Dalrymple, R.W. (Eds.), Principles of Tidal Sedimentology. Springer Netherlands, Dordrecht, pp. 437–471.
Steuber, T., Korbar, T., Jelaska, V., Gušić, I., 2005. Strontium-isotope stratigraphy of Upper cretaceous platform carbonates of the island of Brač (Adriatic Sea, Croatia): implications for global correlation of platform evolution and biostratigraphy. Cretac. Res. 26, 741–756.
Stoll, H.M., Bains, S., 2003. Coccolith Sr/Ca records of productivity during the Paleocene-Eocene thermal maximum from the Weddell Sea. Paleoceanography 18.
Stuart, B.H., Ueland, M., 2017. Decomposition in aquatic environments. In: Taphonomy of Human Remains: Forensic Analysis of the Dead and the Depositional Environment, pp. 235–250.
Sun, Q., Shan, Y., Sein, K., Su, Y., Zhu, Q., Wang, L., Sun, J., Gu, Z., Chu, G., 2016. A 530-year-long record of the Indian summer monsoon from carbonate varves in Maar Lake Twintaung, Myanmar. J. Geophys. Res. Atmos. 121, 5620–5630.
Syme, C.E., Salisbury, S.W., 2014. Patterns of aquatic decay and disarticulation in juvenile Indo-Pacific crocodiles (*Crocodylus porosus*), and implications for the taphonomic interpretation of fossil crocodyliform material. Palaeogeogr. Palaeoclimatol. Palaeoecol. 412, 108–123.
Tarlao, A., Tentor, M., Tunis, G., Venturini, S., 1993. Evidenze di una fase tettonica nel Senoniano inferiore dell'area del Villaggio del Pescatore (Trieste). Gortania Atti Mus. Friul. Stor. Nat. 23–24.
Teather, R.G., 1994. Encyclopedia of Underwater Investigations. Best Pub. Co., Flagstaff, AZ.
Tentor, M., Tunis, G., Venturini, S., 1995. Schema stratigrafico e tettonico del Carso Isontino. Natura Nasc. 9.
Tessier, B., Weill, P., Billeaud, I., Furgerot, L., Campos-Soto, S., Mouazé, D., Caline, B., Bonnot-Courtois, C., 2022. The Bay of Mont Saint Michel: sedimentary facies, morphodynamics and Holocene evolution of a hypertidal coastal system. Geol. Field Trips Maps. 14 (1.2), 39.
Turner, R.E., Baustian, J.J., Swenson, E.M., Spicer, J.S., 2006. Wetland sedimentation from Hurricanes Katrina and Rita. Science 314, 449–452.
Varejão, F.G., Cerri, R.I., Warren, L.V., Rodrigues, M.G., Puetz, S.J., de Lorenso, P.P., Simões, M.G., 2025. Key patterns in exceptional fossil preservation since the rise of metazoans. Earth Sci. Rev. 262, 105065.
Vlahović, I., Tišljar, J., Velić, I., Matičec, D., 2005. Evolution of the Adriatic Carbonate Platform: Palaeogeography, main events and depositional dynamics. Palaeogeogr. Palaeoclimatol. Palaeoecol. 220, 333–360.
Wang, H., Dilcher, D.L., 2018. Early cretaceous angiosperm leaves from the Dakota Formation, Hoisington III locality, Kansas, USA, 21, 1–49.
Wang, B., Ding, Q., 2008. Global monsoon: Dominant mode of annual variation in the tropics. Dyn. Atmos. Oceans 44, 165–183.
Wang, H., Kandasamy, S., Liu, Q., Lin, B., Lou, J.-Y., Veeran, Y., Lei, H., Liu, Z., Chen, C.-T.A., 2021. Roles of sediment supply, geochemical composition and monsoon on organic matter burial along the longitudinal mud belt in the East China Sea in modern times. Geochim. Cosmochim. Acta 305, 66–86.
Wedepohl, K.H., 1971. Environmental influences on the chemical composition of shales and clays. Phys. Chem. Earth 8, 307–333.
Weigelt, J., 1989. Recent Vertebrate Carcasses and their Paleobiological Implications. University of Chicago Press, Chicago, IL.
Woolley, C.H., Bottjer, D.J., Corsetti, F.A., Smith, N.D., 2024. Quantifying the effects of exceptional fossil preservation on the global availability of phylogenetic data in deep time. PLoS One 19, e0297637.
Zhang, K.-J., Li, Q.-H., Yan, L.-L., Zeng, L., Lu, L., Zhang, Y.-X., Hui, J., Jin, X., Tang, X.-C., 2017. Geochemistry of limestones deposited in various plate tectonic settings. Earth Sci. Rev. 167, 27–46.
Ziegler, A.M., Eshel, G., Rees, P.M., Rothfus, T.A., Rowley, D.B., Sunderlin, D., 2003. Tracing the tropics across land and sea: Permian to present. Lethaia 36, 227–254.